Chapter-4

Magnetic Properties of FePtCo Ternary Alloy Thin Films

Chapter-4

Magnetic Properties of FePtCo Ternary Alloy Thin Films

In this chapter the magnetic properties of FePtCo ternary alloy thin films prepared under different deposition conditions are discussed. The chapter consists mainly of discussion of four measurement results namely compositional analysis by SEM-EDS, surface topography and film surface roughness measurement by 3D optical profilometer and atomic force microscopy, crystal structural analysis by grazing incidence x-ray diffraction technique and magnetic properties measurement by vibrating sample magnetometer. A brief description of sample fabrication process is also included in this chapter. The film surface roughness measurement results, structural analysis and magnetic property measurement results each are discussed separately for each deposition condition. Then the obtained results for each deposition conditions are compared to discuss the influence of different deposition conditions.

The results discussed in the current chapter have been published in journal in reference [235].

4.1 Fabrication of FePtCo Ternary Alloy Thin Films

The $(Fe_{0.4}Pt_{0.6})_{1-x}Co_x$ ternary alloy thin films were grown on Si wafer of 2 inch diameter and 1 mm thickness using a magnetron sputtering system by co-sputtering of pure Co target with $Fe_{40}Pt_{60}$ alloy target. Before deposition, the Co, $Fe_{40}Pt_{60,}$ and Cu targets were loaded onto the magnetron sputtering chamber. The sputtering chamber was then evacuated with the help of a rotary vane pump as roughing pump and a diffusion pump to a pressure of 5 mTorr. Then Ar gas was introduced into the vacuum chamber as a sputtering gas. The Ar gas flow was maintained at a constant flow rate of 10 sccm and target sputtering power was gradually increased by increasing target voltage and ion current to desired values. The $Fe_{40}Pt_{60}$ target was sputtered at constant power of 25 watt and the Co target was sputtered at five different powers 0, 25, 50, 75 and 100 watt to obtain five thin film samples of varying Co content of the thin films. Before the actual deposition of the films deposition rate i.e., thickness deposited per minute was determined. Then the actual films were deposited in such a way as to maintain the same thickness of ∼100 nm of each film by maintaining the desired deposition time.

The samples were deposited under three different conditions: first, actual films were deposited on a substrate at room temperature called “as-deposited”, second, the substrates were heated at temperature 673 K, held at temperature, and films were deposited on the heated substrates at that temperature and is called “in-situ annealing” and the third, a nonmagnetic element Cu of thickness of 2 nm called underlayer was deposited first on the substrate at room temperature, then the actual films were deposited on the underlayer and is called as “Cu-underlayered”. In all three conditions, the other sputtering parameters such as Ar gas flow, Co target sputtering powers were maintained same. Thus first two sets consist of four FePtCo samples along with pure $Fe_{40}Pt_{60}$ alloy film, a total of five samples in each set. The Cu-underlayered set of samples consists of four FePtCo alloy films. Thus a total of fourteen FePtCo ternary alloy thin films of varying Co content were prepared.

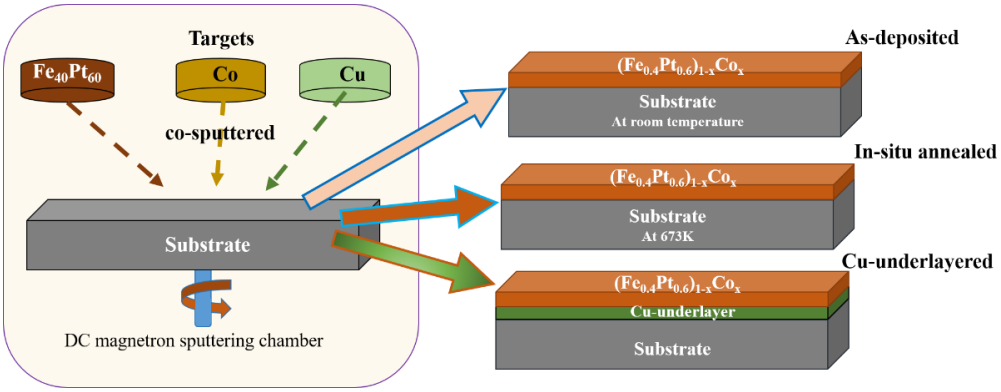

Figure 4.1 Schematic representation of co-sputtering of FePt and Co under three deposition conditions.

4.2 Optimization of Deposition Rate of Each Target

One of the primary tasks before the deposition of actual thin films is to optimize the deposition rate of each target to be used for deposition. The target material must be sputtered at a particular sputtering power at which the maximum deposition yield is obtained and the thin film is uniformly deposited. Each of the two targets $Fe_{40}Pt_{60}$ and pure Co elemental targets used in the deposition of FePtCo thin film was sputtered at three different sputtering powers, one at which bright plasma is produced and the other two greater by 5 watt and 10 watt, maintaining the same vacuum pressure $3x10^{-2}$ mbar. The deposition pressure was adjusted by Ar gas flow and deposited for one hour. The uniformity of film deposited by each target was checked using Profilm 3D optical profilometer. For $Fe_{40}Pt_{60}$ and Co target, uniform films of sufficient thickness were deposited at 25 watt and hence 25 watt was selected for sputtering the actual film. To vary the composition of films, Co target was sputtered at four different powers namely 25, 50, 75, and 100 watt and $Fe_{40}Pt_{60}$ target sputtered at fixed power of 25 watt. To determine the overall deposition rate and hence the overall thickness of the thin film, the films were deposited on a partially masked substrate for 30 minutes. The masks were removed after deposition and the step height formed was measured by step height measurement mode using 3D optical profilometer. The same process is repeated three times and the average deposition rate per minute is determined for each target at specified sputtering power. One typical step height deposited and step height measurement

of the film with $Fe_{40}Pt_{60}$ target deposited at 25 watt and Co at 75 watt for optimization of deposition rate and actual film deposited are presented in top panel and bottom panel of Figure 4.2 respectively. The average deposition rate per minute against each sputtering power is presented in Table 4.1. The actual thin films were then deposited for the desired duration (Table 4.1) to maintain approximately the same thickness of 100 nm for all the prepared thin films.

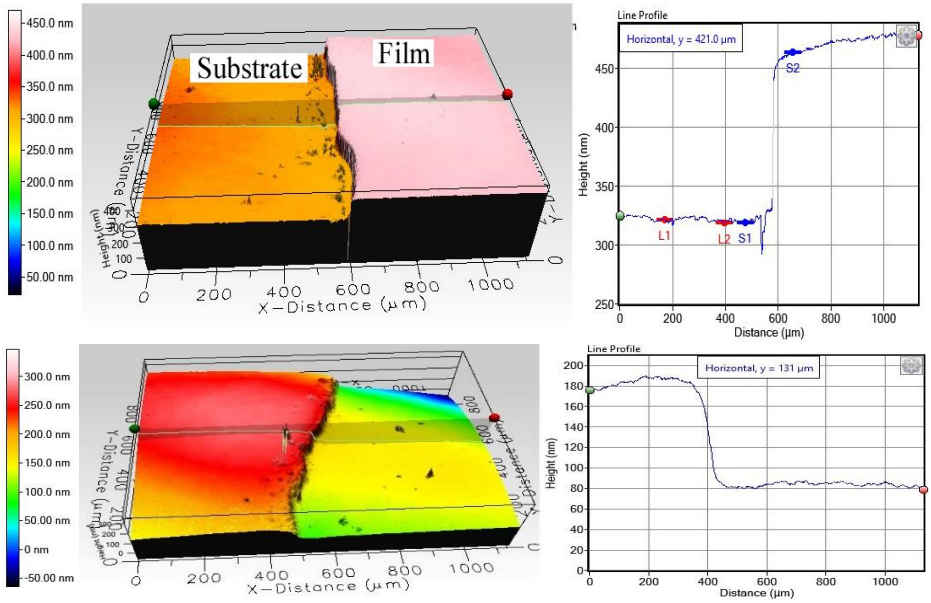

Figure 4.2 Typical 3D image along with colour contrast z-scale and line profile of sample with $Fe_{40}Pt_{60}$ and Co target deposited at 25 and 75 watt respectively for optimization of deposition rate (top panel) and actual film (bottom panel).

Table 4.1 Deposition rate, deposition time and thickness of actual thin films sputtered at different powers.

Sample	Sputtering power (watt)		Deposition rate (nm/min)	Deposition time (minute)	Thickness (nm) (approx.)
$(Fe_{0.4}Pt_{0.6})_{1-x}Co_x$	$Fe_{40}Pt_{60}$	Co			
Sample-1	25	0	3.32	30	100
Sample-2	25	25	3.70	27	100
Sample-3	25	50	4.06	25	100
Sample-4	25	75	4.76	21	100
Sample-5	25	100	6.25	16	100

4.3 Compositional Analysis by EDX

For compositional analysis by EDX, the deposited samples were cut into small pieces (4mm x 4mm approx.). The cut pieces of samples were then attached to the sample holder with the help of a carbon tap and then gold coated to facilitate conductive path for electrons. After the samples were gold coated, the samples were loaded into the vacuum chamber of SEM equipped with EDX. The vacuum chamber is evacuated with the help of turbo molecular pump (TMP) to a vacuum pressure of order 10^{-7} mbar. The unwanted elements appearing in the EDX spectra due to substrate, gold coating, carbon tape, etc. were removed keeping only the three elements Fe, Pt and Co. The obtained EDX spectra of Co-doped FePt thin films are presented in Figure 4.3. The prepared ternary alloy thin films are designated by $(Fe_{0.4}Pt_{0.6})_{1-x}Co_x$ and the compositions of the films are measured in relative atomic percentage. The obtained compositions of the thin films are presented in Table 4.2. The Co content of the films increases with the increase in sputtering power of Co target as expected.

Table 4.2 Composition of FePtCo ternary alloy thin films obtained from EDX spectrum.

Sample	Target	Sputtering power (Watt)	Atomic percentage			Composition $(Fe_{0.4}Pt_{0.6})_{1-x}Co_x$
			Fe	Pt	Co	
1	$Fe_{40}Pt_{60}$	25	36.23	53.01	10.76	$(Fe_{0.4}Pt_{0.6})_{0.89}Co_{0.11}$
	Co	25				
2	$Fe_{40}Pt_{60}$	25	31.85	50.92	17.23	$(Fe_{0.4}Pt_{0.6})_{0.83}Co_{0.17}$
	Co	50				
3	$Fe_{40}Pt_{60}$	25	29.61	42.64	27.75	$(Fe_{0.4}Pt_{0.6})_{0.72}Co_{0.28}$
	Co	75				
4	$Fe_{40}Pt_{60}$	25	28.10	41.54	30.36	$(Fe_{0.4}Pt_{0.6})_{0.70}Co_{0.30}$
	Co	100				

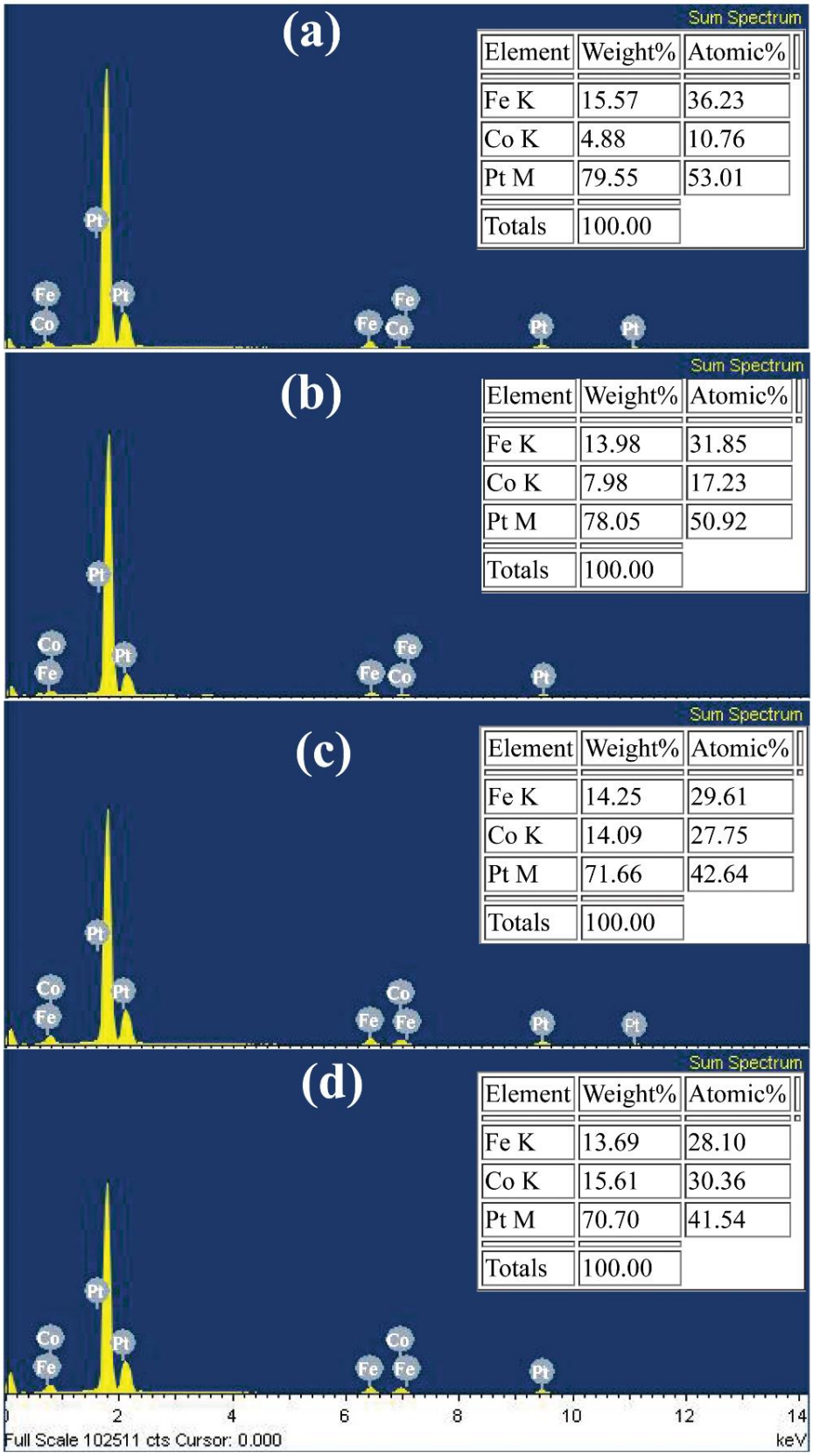

Figure 4.3 EDX spectra of FePtCo ternary alloy thin films with Co deposited at (a) 25, (b) 50, (c) 75 and (d) 100 watt.

4.4 Film Surface Roughness Measurement by Optical Profilometer

The surface topography and the film surface roughness have been measured using Profilm 3D optical profilometer. The measurement was carried out by using phase shifting interferometry (PSI) mode of scan. The film surface is captured by an integrated 4x Nikon DI objective lens. The $200\ \mu m \times 200\ \mu m$ area of the sample was selected and then S_a and R_a of the sample surface were measured in ISO 25178 Height and ISO 4287 Amplitude standards respectively. S_a is the arithmetic mean or the average of the absolute distances of the surface points from the mean plane [212]. The digital equation by which S_a [212] is measured by

$$S_a = \frac{1}{MN}\sum_{j=1}^{N}\sum_{N=1}^{M}|z|(x_i, y_j) \tag{4.1}$$

Where, M is the number of columns in the surface and N is the number of rows in the surface. The R_a on the other hand is arithmetic mean of absolute ordinate values Z(x) within the sampling length [185]. The equation by which R_a [185] is measured is

$$R_a = \frac{1}{l}\int_0^l |Z(x)|dx \tag{4. 2}$$

Where l is the sampling length.

4.4.1 Surface Topography and Surface Roughness of As-deposited FePtCo Films

The coloured 3D image of surface topography (middle panel) with colour contrast z-scale (left panel) and line profile (right panel) of the as-deposited thin films are presented in Figure 4.4. The colour contrast of the film gives a qualitative indication of the film surface roughness and the 3D image indicates the film surface quality.

The value of R_a varies along different lines of the scanned sample. So for the best result, the R_a is measured along the middle of the sample. The measured values of S_a and R_a are presented in Table 4.3, and are plotted as a function of film composition in Figure 4.6. S_a of the as-deposited films are found to decrease gradually with an increase in Co-doping from 1.41 nm for undoped FePt film to 0.76 nm for 28 at. % Co-doped FePt film, thereafter sudden increase to 2.48 nm is observed for 30 at. % Co-doped film. The sudden increase in S_a is attributed to the high sputtering power of Co target due to which energetic Co atoms are deposited on substrate more randomly. On the other hand the as-deposited films possess smaller R_a than S_a as expected, and slightly vary with film composition in the range of 0.47 nm to 0.66 nm. The observed values of S_a and R_a are very small relative to the film thickness of 100 nm. This indicates that the deposited films are sufficiently smooth. The surface topography and roughness R_a were also measured using AFM. The 2D and 3D view of AFM images of are presented in Figure 4.5 and the measured values of R_a are presented in Table 4.3. The R_a varies with film composition in the range of 0.41 nm to 1.57 nm. The R_a increases linearly with an increase in Co-doping upto 17 at. % as depicted in Figure 4.6. For 28 at. % Co-doped film, slightly smaller R_a is observed and with further increase in Co-doping to 30 at. % sudden increase in R_a is observed.

Table 4.3 Measured values of S_a and R_a measured by both 3D optical profilometer and AFM of as-deposited FePtCo thin films.

Sample	$(Fe_{0.4}Pt_{0.6})_{1-x}Co_x$	x=0	x=0.11	x=0.17	x=0.28	x=0.30
As-deposited	S_a (nm)	1.41	1.11	0.81	0.76	2.48
	R_a (nm)	0.53	0.47	0.48	0.52	0.66
	R_a (nm) (AFM)	0.41	0.53	0.68	0.46	1.57

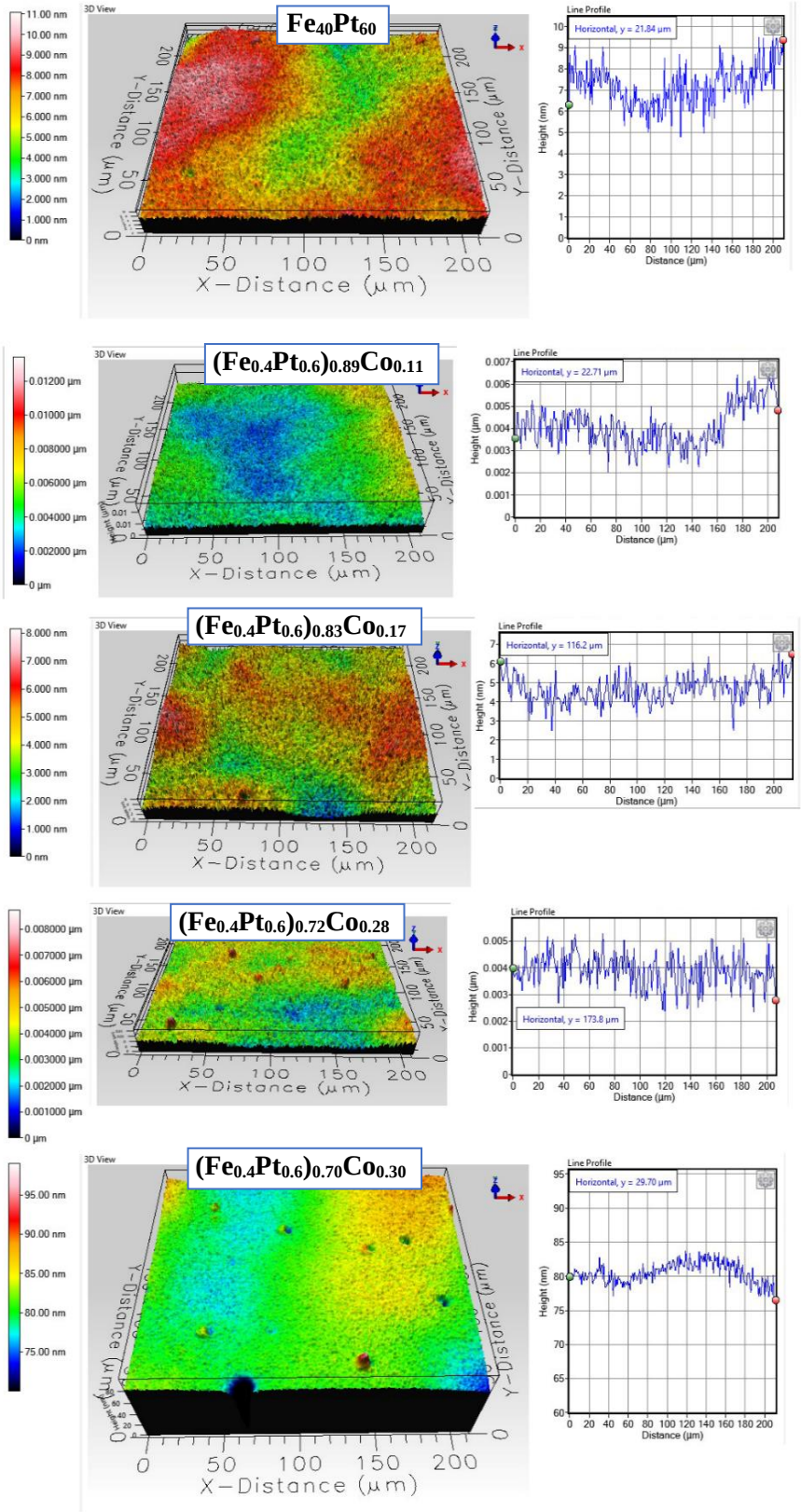

Figure 4.4 Coloured 3D image (middle) and line profile (right) along with colour contrast z-scale (left) of as-deposited FePtCo ternary alloy thin films.

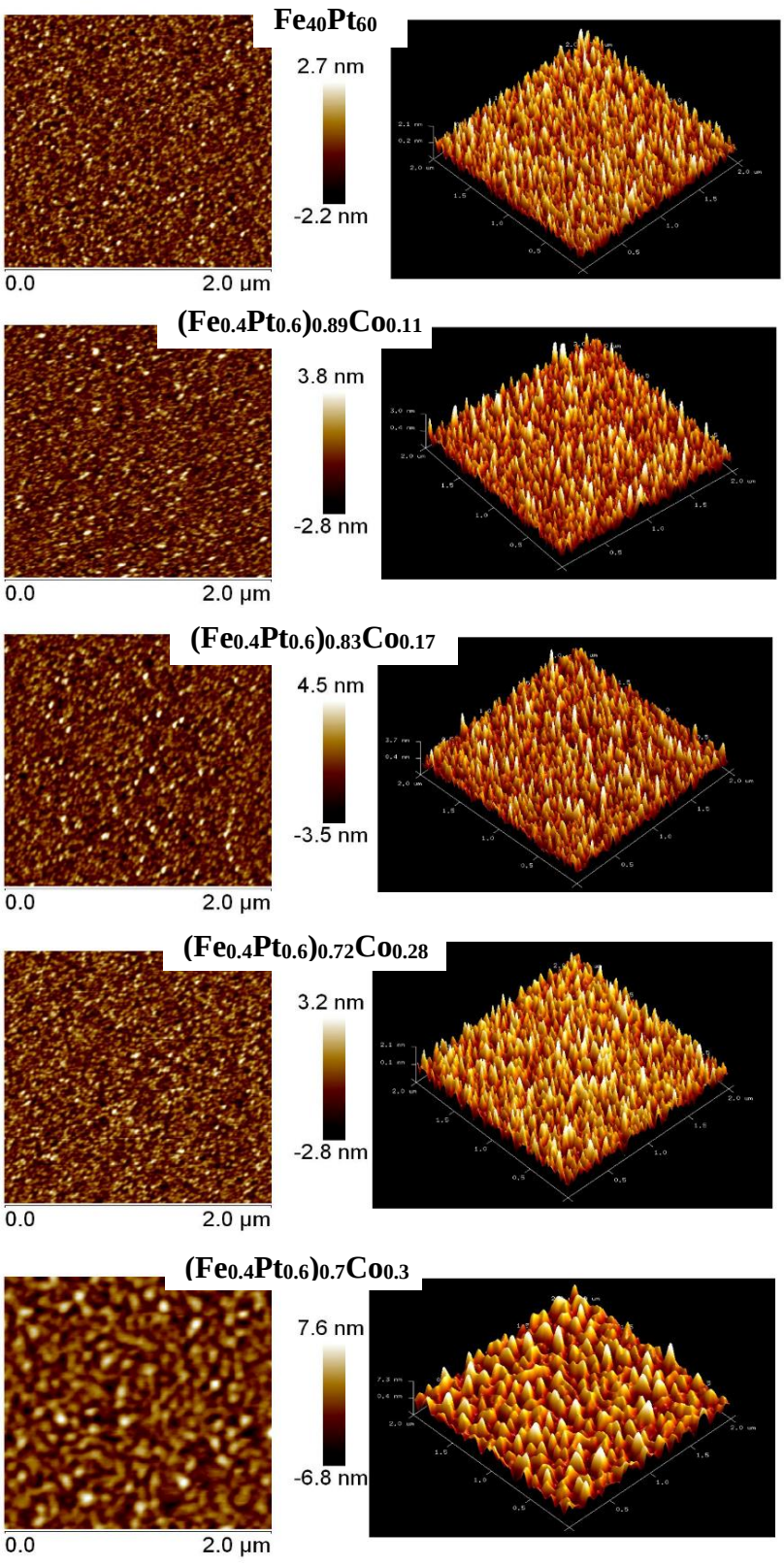

Figure 4.5 2D and 3D AFM image of as-deposited FePt and FePtCo alloy thin films.

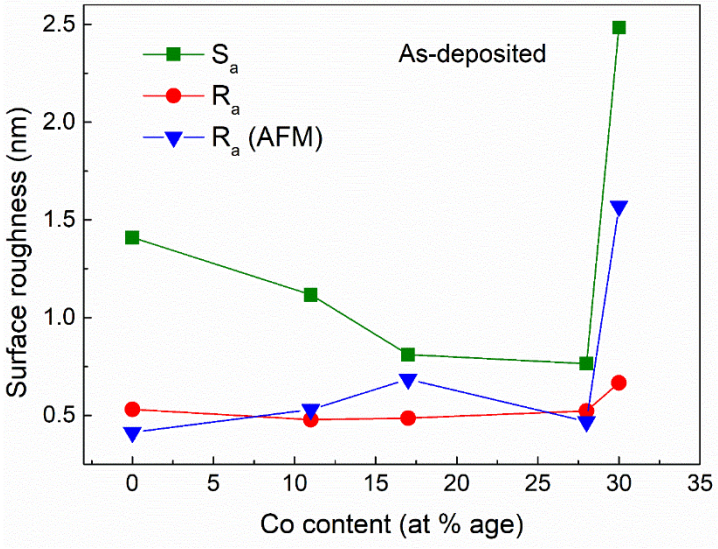

Figure 4.6 Plot of S_a, R_a obtained from 3D optical profilometer, and R_a obtained by AFM as a function of Co content of as-deposited FePtCo films.

4.4.2 Surface Topography and Surface Roughness of in-situ annealed FePtCo Thin Films

The coloured 3D image of surface topography (middle panel) with colour contrast z-scale (left panel) and line profile (right panel) of the in-situ annealed thin films measured by 3D optical profilometer are presented in Figure 4.7. The colour contrast of the films gives a qualitative indication of the film surface roughness and the 3D image indicates the film surface quality. The value of R_a varies when measured along different lines within the scanned area of sample as usual. So for the best result, the R_a is measured along a line in the middle of the sample. The measured values of S_a and R_a are presented in Table 4.4 and are plotted as a function of Co-doping content of the films in Figure 4.9. From Figure 4.9, it is seen that S_a first decreases with Co doping from 1.02 nm for pure FePt film to 0.83 nm for 11 at. % Co. With further increase of Co content beyond 11 at. %, the S_a increases to 1.06 nm with an increase in Co addition to 30 at. %. The R_a obtained by optical profilometer shows a small variation in the range of 0.48 nm to 0.54 nm with Co addition to FePt alloy. These values of R_a are found to be smaller than the values of S_a as usual for corresponding films with the same composition. However, the R_a obtained by AFM shows a gradual increase with Co addition from 0.23 nm for pure FePt film to 0.64 nm for 28 at. % Co. These values are also found to be smaller than

the values of S_a obtained by an optical profilometer. These observed values of S_a and R_a indicate that the prepared thin films are relatively smooth.

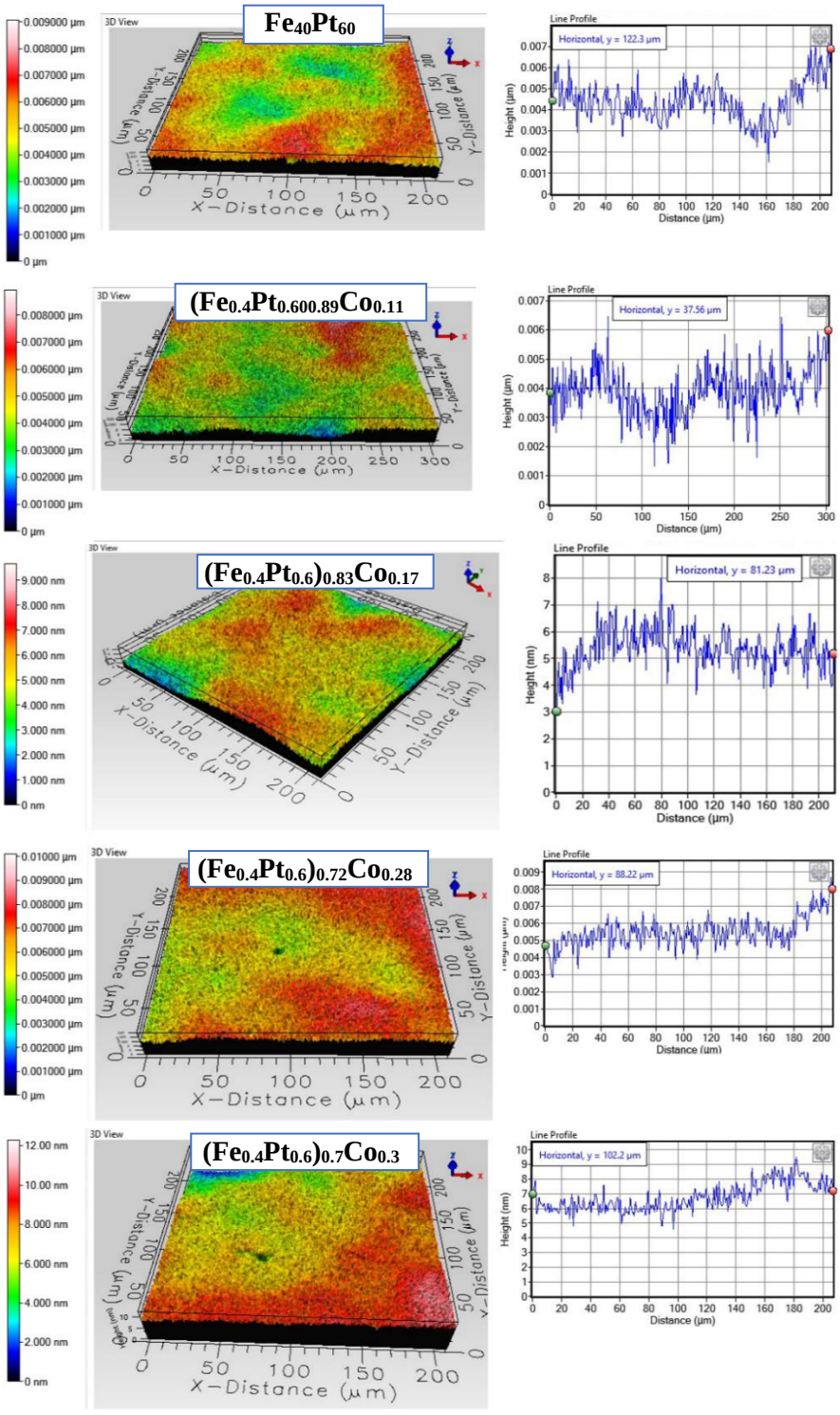

Figure 4.7 3D image of film surface (middle), colour contrast z-scale (left) and line profile (right) of in-situ annealed FePt and FePtCo alloy thin films.

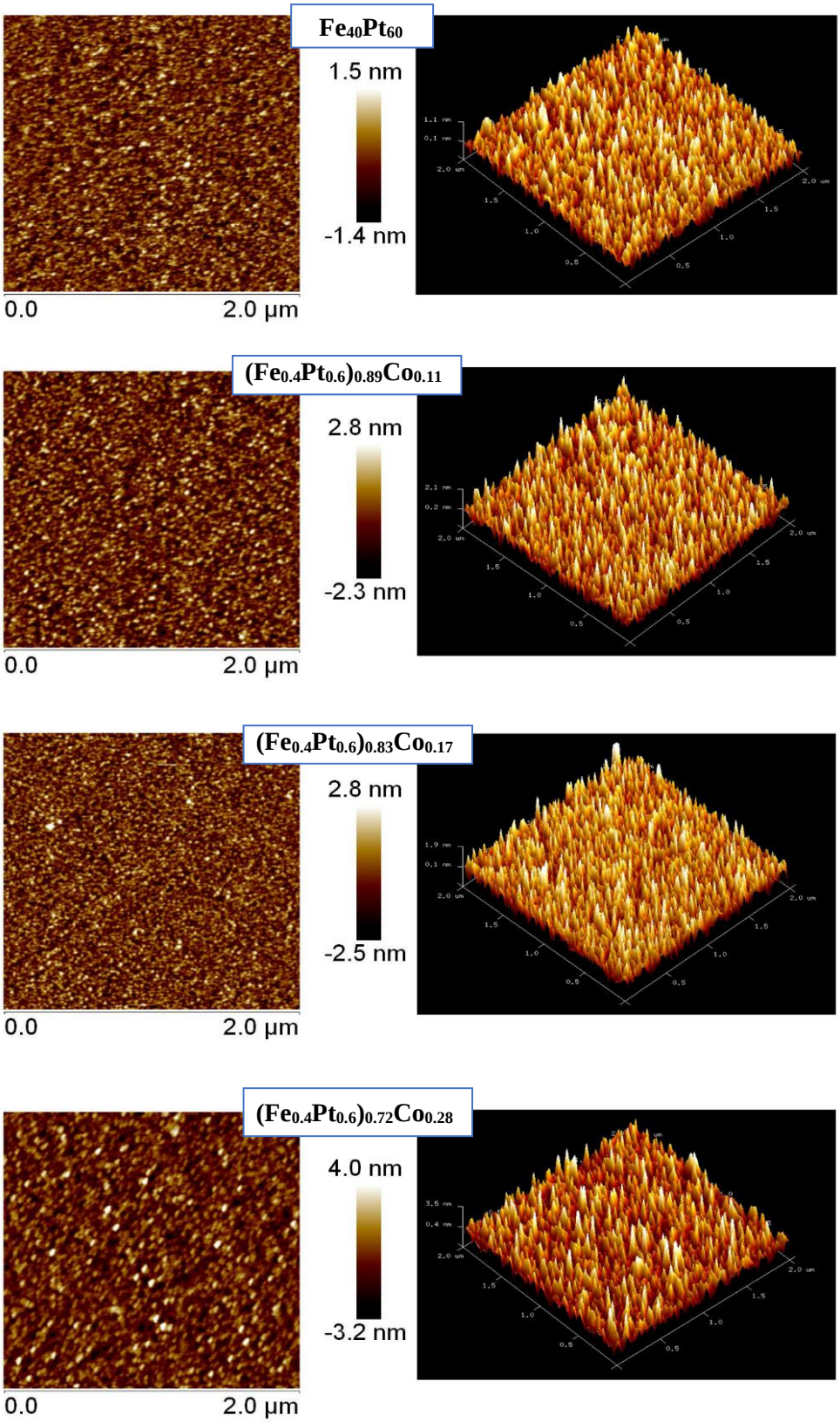

Figure 4.8 2D and 3D AFM image of in-situ annealed FePt and FePtCo alloy thin films.

Table 4.4 Surface roughness parameters S_a and R_a measured by 3D optical profilometer and AFM.

Sample	$(Fe_{0.4}Pt_{0.6})_{1-x}Co_x$	x=0	x=0.11	x=0.17	x=0.28	x=0.30
in-situ annealed	S_a (nm)	1.02	0.83	0.91	0.97	1.06
	R_a (nm)	0.53	0.54	0.48	0.49	0.52
	R_a (nm) (AFM)	0.23	0.44	0.40	0.64	-

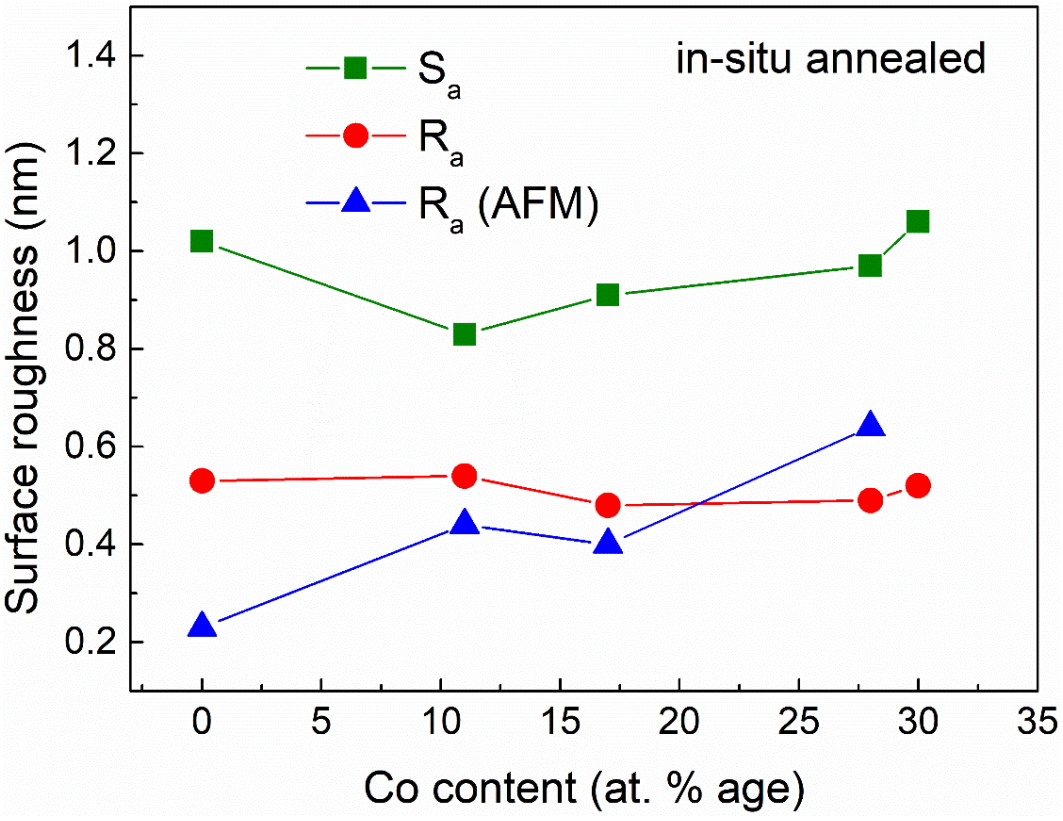

Figure 4.9 Plot of S_a (black) and R_a (red) obtained using 3D optical profilometer, and R_a (blue) obtained by AFM a function of film composition of in-situ annealed FePtCo alloy thin films.

4.4.3 Surface Topography and Surface Roughness of Cu-underlayered FePtCo Thin Films

The coloured 3D image of surface topography (middle panel) with colour contrast z-scale (left panel) and line profile (right panel) of the FePtCo thin films with Cu-underlayer are presented in Figure 4.10. The colour contrast of the film gives a qualitative indication of the film surface roughness and the 3D image indicates the film surface quality. The value of R_a varies along different lines of the scanned sample. So for the best result, the R_a was measured along the middle of the sample. The measured values of S_a and R_a are presented in Table 4.5 and are plotted as a function of Co-doping concentration in Figure 4.12. A slight decrease in S_a is observed from 0.84 nm for x=0.11 to 0.76 nm for x=0.17. However, with further increase in Co content overall increase in S_a is observed as shown in Figure 4.12. The R_a obtained by the optical profilometer also shows an overall increase with an increase in Co addition to the FePt film. The R_a values are also smaller than the S_a of corresponding samples which is consistent with the results of as-deposited and annealed samples. The R_a obtained by AFM also shows a similar trend as that of S_a obtained by optical profilometer showing an overall increase with an increase in Co addition as depicted in Figure 4.12. A clear indication of increasing roughness can be observed in the AFM image (Figure 4.11), due to the formation of particulate on the film surface.

Table 4.5 Surface roughness S_a and R_a of FePtCo films with Cu-underlayer measured by 3D optical profilometer and AFM.

Sample	$Cu/(Fe_{0.4}Pt_{0.6})_{1-x}Co_x$	x=0.11	x=0.17	x=0.28	x=0.30
Cu-underlayered	S_a (nm)	0.84	0.76	1.25	1.03
	R_a (nm)	0.41	0.41	0.54	0.44
	R_a (nm) (AFM)	0.50	0.36	0.92	0.92

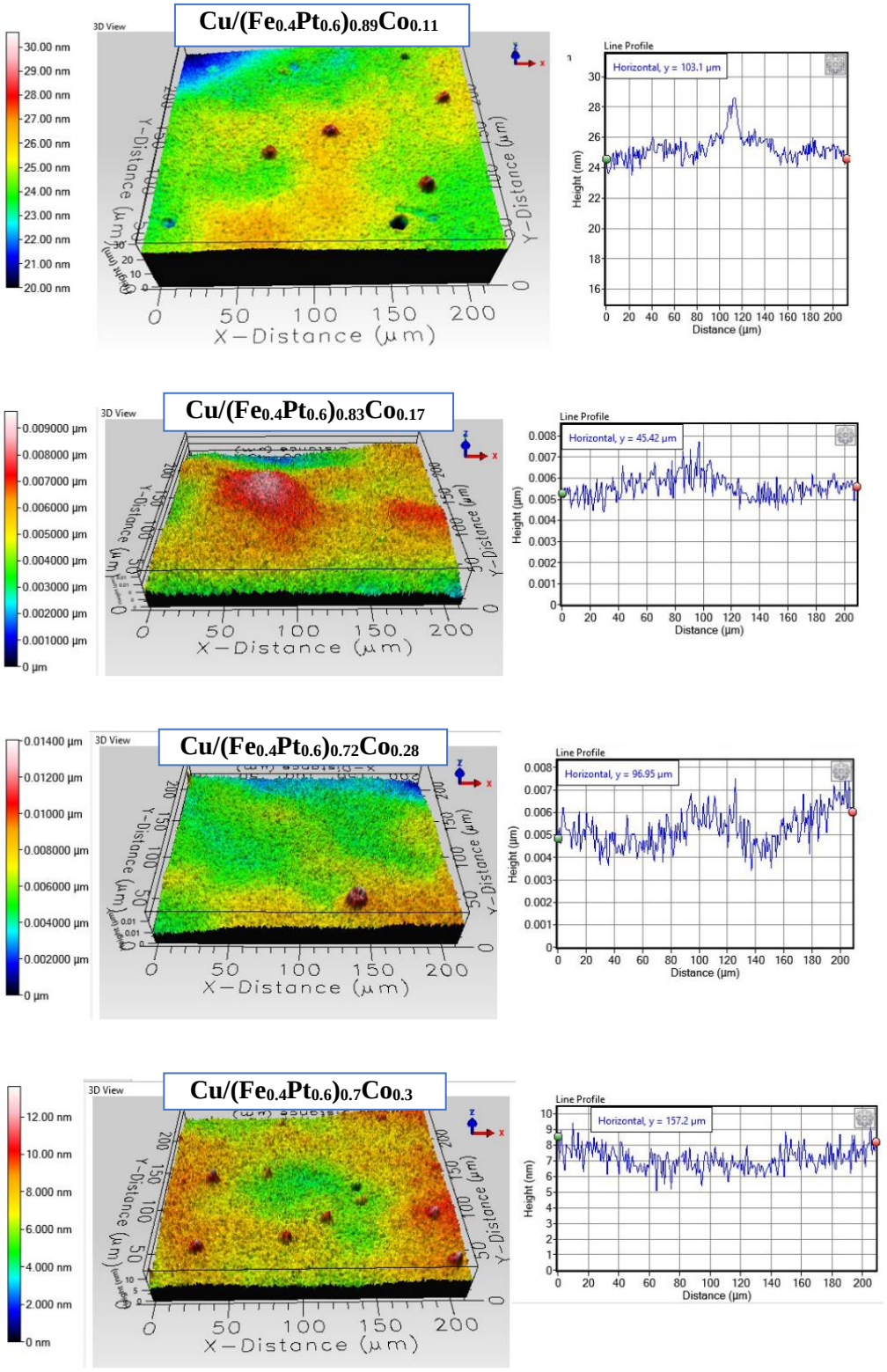

Figure 4.10 3D image of film surface (middle), colour contrast z-scale (left) and line profile (right) of FePtCo alloy thin films with Cu-underlayer.

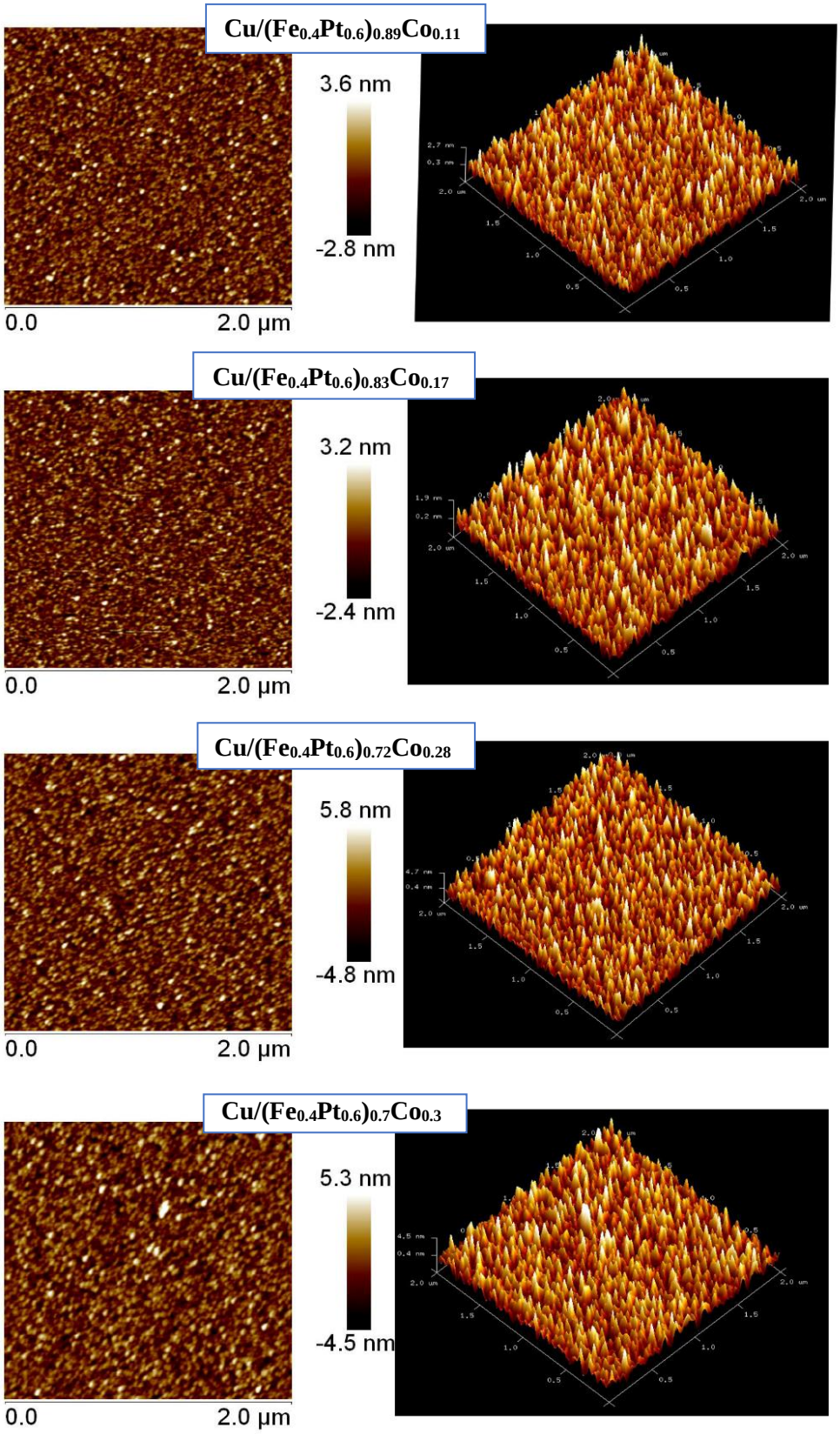

Figure 4.11 2D and 3D AFM image of Cu-underlayered FePtCo alloy thin films.

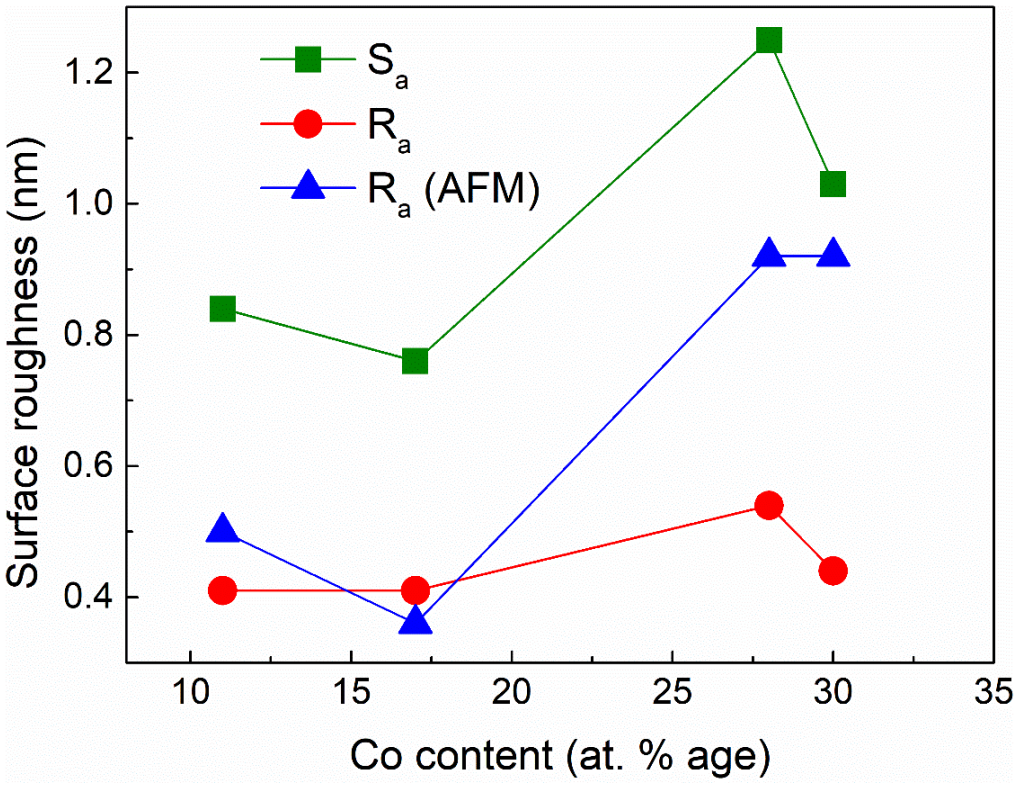

Figure 4.12 Plot of film surface roughness of Cu-underlayered FePtCo films obtained by optical profilometer and AFM.

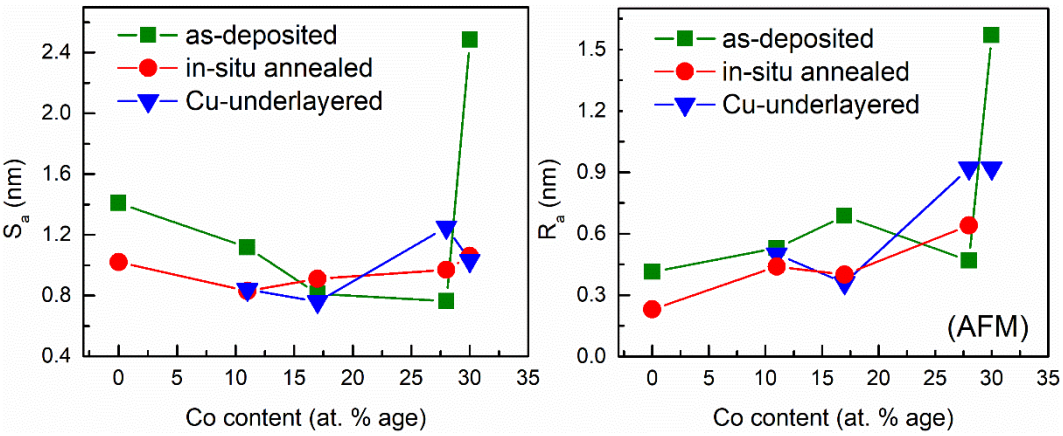

Figure 4.13. Comparative plot of S_a obtained by optical profilometer (left) and R_a obtained by AFM (right) of all prepared FePtCo thin films.

For a comparative study of the surface roughness of all FePtCo thin films prepared under the three conditions, a comparative plot of S_a obtained by optical profilometer and Ra obtained by AFM has been presented in Figure 4.13. From Figure 4.13, it is noticed that S_a of all prepared thin films first decreases with an increase in Co

content up to 17 at. % Co and thereafter overall increase is observed. The annealed and Cu-underlayered films possess smaller film surface roughness S_a than as-deposited films. The AFM results show an overall increase of R_a with the increase in Co content of all films. The AFM results also indicate that the annealed and Cu-underlayered thin films possess smaller surface roughness than as-deposited films as depicted in Figure 4.13.

4.5 X-ray Diffraction Measurement Results

4.5.1 Room Temperature XRD Results of as-deposited FePtCo Thin Films

For structural analysis, X-ray diffraction (XRD) measurement was carried out for all samples at room temperature. The Co K_α radiation with $\lambda = 1.79$ Å was used in the XRD measurement. The obtained XRD results of all as-deposited FePtCo thin films are presented in Figure 4.14. The phase of the thin films was identified using Xpert High Score Plus software and found that all as-deposited thin films exhibit the face-centered cubic structure with space group $Fm\bar{3}m$ No. 225. The two prominent XRD peaks are identified as the reflection from (111), and (220) plane and a low intensity peak as (200). All these three peaks correspond to FCC phase [94,121,124,127,133,236]. No other XRD peak has been observed in the XRD pattern. This indicates that the samples are of a single phase. A slight shifting of XRD peaks in higher 2θ positions is observed with an increase in Co addition. This indicates that the lattice parameters decrease with an increase in Co doping which is evident due to the smaller atomic radius of Co than Pt. To determine the lattice parameters, Rietveld refinement of the XRD pattern has been carried out using FullProf Suite software [237–239] using the pseudo-voight peak function. The Rietveld refinement fit of XRD profile of as-deposited films are presented in Figure 4.14 and obtained parameters are listed in Table 4.6. The obtained results indicate that the unit cell parameters decrease from 3.82 Å for pure FePt film with an increase Co doping to 3.74 Å for 30 at. % Co doping. The variation of lattice parameters as a function of at. % age of Co content is plotted in Figure 4.15. The

result indicates that Co addition to FePt reduces the unit cell parameters. However, the crystal structure of all Co doped as-deposited films remains same.

Table 4.6 Lattice parameters obtained from Rietveld refinement and goodness of fitting, χ^2, and average crystallite size of as-deposited films.

Sample	$(Fe_{0.4}Pt_{0.6})_{1-x}Co_x$	x=0	x=0.11	x=0.17	x=0.28	x=0.30
as-deposited	Lattice parameters, a=b=c (Å)	3.82	3.80	3.79	3.76	3.74
	χ^2	1.40	1.29	1.23	1.38	1.24
	Crystallite size (nm)	21.4(3)	15.7(1)	10.8(5)	13.0(8)	13.0(5)
	Adj. R^2	0.99	0.98	0.99	0.99	0.99

To calculate the average crystallite size, the highest intensity XRD peak (111) is fitted by the pseudo-voigt peak function. The fitting parameters such as FWHM, peak position, and standard deviation are obtained and the average crystallite size of the films is calculated using Debye Scherrer equation [2340,242].

$$D_v = \frac{k\lambda}{\beta \cos\theta} \tag{4. 3}$$

Where $k = 0.9$ is a constant, $\lambda(= 1.79$ Å) is the wavelength of the x-ray (Co-K_α), β is FWHM of XRD peak and θ is obtained by dividing peak position (2θ) by 2. The obtained average crystallite size of all as-deposited films is presented in Table 4.6 and the variation of average crystallite size has been plotted as a function of Co-content of the samples and presented in Figure 4.15. It is seen that the average crystallite size decreases with an increase in Co doping from 21 nm for pure FePt film to 11 nm for 17 at. % Co doped film. With further Co doping the average crystallite size of the films again increases to 13 nm resulting a nonlinear variation.

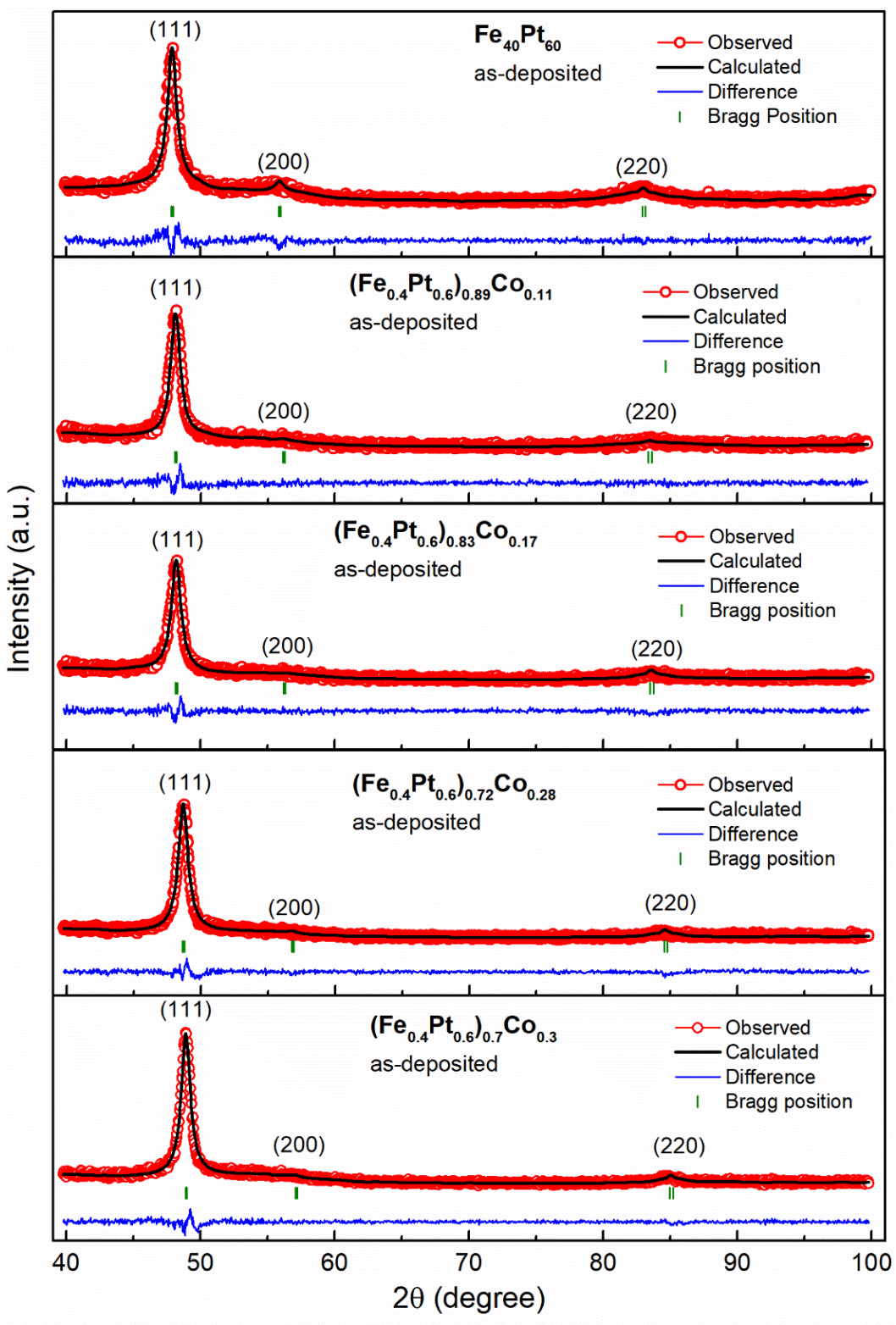

Figure 4.14 Room temperature XRD profile along with Rietveld refinement fit of as-deposited FePtCo thin films.

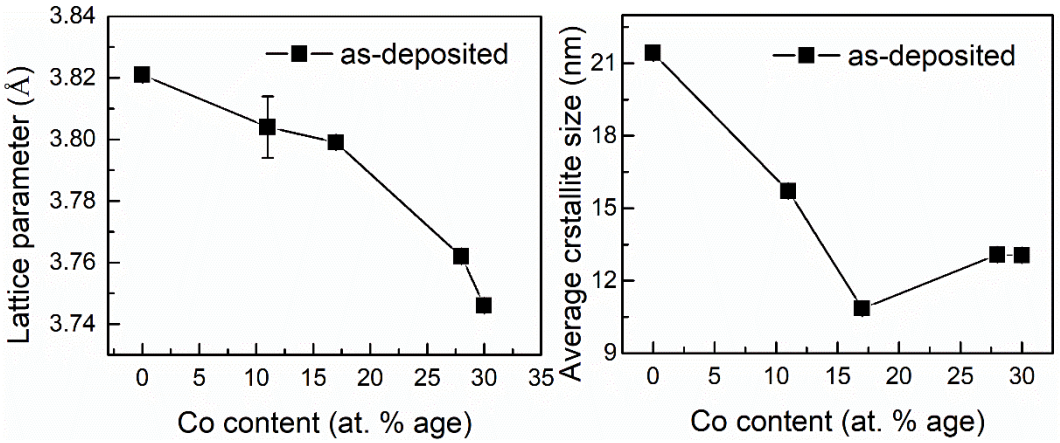

Figure 4.15 Plot of lattice parameter (left) and average crystallite size of as-deposited FePtCo films as a function of Co content of the films.

4.5.2 Room Temperature XRD Results of In-situ Annealed FePtCo Thin Films

The crystal structures of in-situ annealed thin films are also analyzed using X-ray diffraction (XRD) measurement. The Co K_α radiation with $\lambda = 1.79$ Å was used in the XRD measurement. The obtained XRD profile of in-situ annealed FePtCo thin films is presented in Figure 4.16. The phase of the thin films was identified using Xpert High Score Plus software and found that all in-situ annealed thin films also exhibit the face-centered cubic structure with space group $Fm\bar{3}m$ No. 225. The XRD peaks are identified as reflection from (111), (200) and (220) plane respectively. All these three peaks correspond to the FCC phase [94,121,124,127,133,236] and no other XRD peak has been observed in the XRD pattern which indicates that all samples are of a single phase. With an increase in Co content of films, shifting of XRD peaks of annealed films have been observed in higher 2θ positions except 17 at. % Co doped film. This shows that the lattice parameters decrease with an increase in Co content of the films. However, for 17 at. % Co doped film XRD peaks shift towards lower 2θ positions and a large broadening of peaks is observed. To determine the lattice parameters, Rietveld refinement of the XRD pattern has been carried out using FullProf Suite software [237–239] using the pseudo-voigt peak function. The Rietveld refinement fit of XRD profile of annealed films is presented in Figure 4.16 and obtained

parameters are listed in Table 4.7. The overall decrease in lattice parameters is observed with an increase in Co doping from 3.81 Å for pure FePt film to 3.74 Å for 30 at. % Co-doped film as shown in Figure 4.17. However, due to large peak broadening for 17 at. % Co doped film, the lattice parameter could not be determined correctly and a larger lattice parameter than other annealed films is found from Rietveld refinement as depicted in Figure 4.17 (left). To calculate average crystallite size, the highest intensity XRD peak (111) is fitted by the pseudo-voigt peak function. The fitting parameters such as FWHM and peak position are then used to calculate average crystallite size using Debye-Scherrer equation (4. 3). Due to the large peak broadening of annealed film with Co 17 at. %, the XRD peak could not be fitted and hence crystallite size could not be determined. The obtained average crystallite size of all prepared films is presented in Table 4.7 and the variation of average crystallite size of the as-deposited films have been plotted as a function of Co content of the films in Figure 4.17. The average crystallite size is found to first increase with Co doping from 14.44 nm for pure FePt film to 17.71 nm for 11 at. % Co. On further increase in Co doping beyond 11 % the crystallite size again decreases to 9.88 nm for 30 at. % Co.

Table 4.7 Lattice parameters obtained from Rietveld refinement and goodness of fit (χ^2), and average crystallite size of in-situ annealed films.

Sample	$(Fe_{0.4}Pt_{0.6})_{1-x}Co_x$	x=0	x=0.11	x=0.17	x=0.28	x=0.30
In-situ annealed	Lattice parameters, a=b=c (Å)	3.81	3.80	3.90	3.75	3.74
	χ^2	1.69	1.20	1.18	1.94	1.29
	Crystallite size (nm)	14.4(4)	17.7(1)	-	11.5(7)	9.8(8)
	Adj. R^2	0.98	0.98	-	0.99	0.98

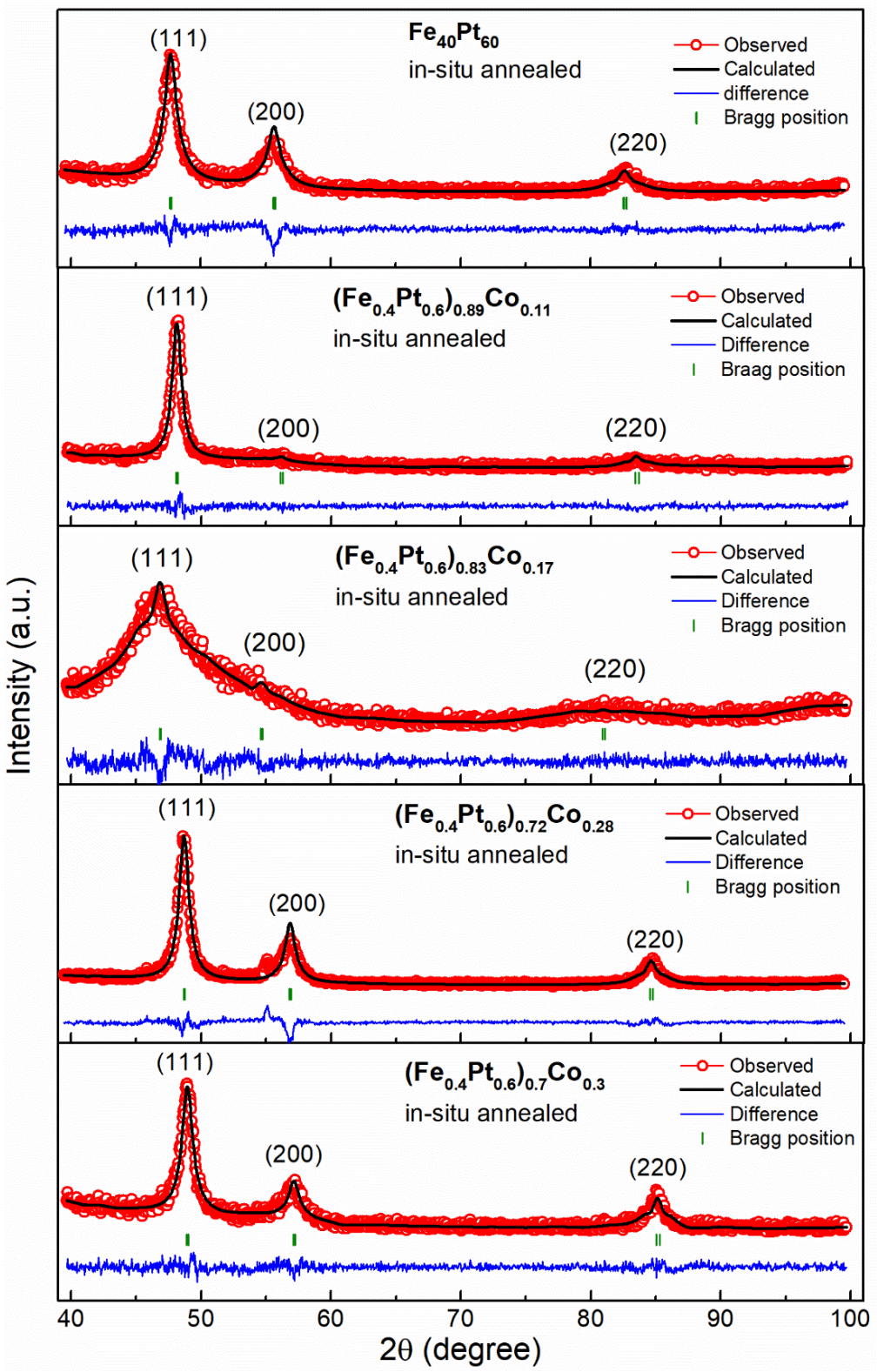

Figure 4.16 Room temperature XRD profile along with Rietveld refinement fit of in-situ annealed FePtCo thin films.

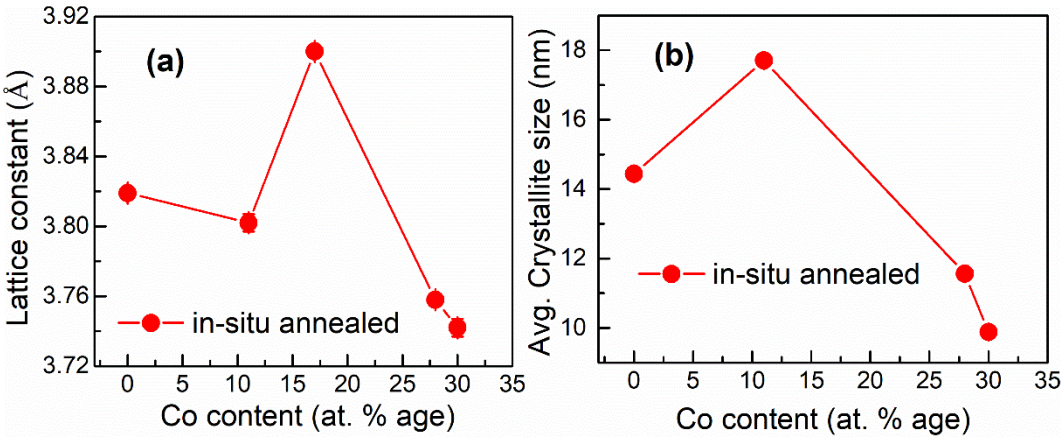

Figure 4.17 Plot of lattice parameter (left) and average crystallite size of in-situ annealed FePtCo films as a function of Co content of the films.

4.5.3 Room Temperature XRD Results of Cu-underlayered FePtCo Thin Films

The room temperature XRD profile along with the Rietveld refinement fit of Cu-underlayered FePtCo thin films are presented in Figure 4.18. The phase of the thin films was identified using Xpert High Score Plus software and found that all Cu-underlayered thin films also exhibit the face-centered cubic structure with space group $Fm\bar{3}m$ No. 225. The XRD peaks are identified as reflection from (111), (200), and (220) plane respectively. All these three peaks correspond to the FCC phase [94,121,124,127,133,236] and no other XRD peak has been observed in the XRD pattern which indicates that all samples are of a single phase. With the increase in Co content of films, shifting of XRD peaks of annealed films have been observed in higher 2θ positions indicating that the lattice parameters decrease with an increase in Co content of the films. The lattice parameters obtained by Rietveld refinement fit using FullProf Suite software are presented in Table 4.8. With increase in Co doping from 11 to 30 at. %, decrease in lattice parameter from 3.79 Å to 3.75 Å has been observed. The average crystallite size of Cu-underlayered films is also calculated similarly by fitting the highest intensity XRD peak (111) to the pseudo-voigt peak function. The fitting parameters such as FWHM and peak position are then used to calculate the average crystallite size using Debye-Scherrer equation (4. 3). The obtained average crystallite size of all prepared films are presented in Table 4.8 and the variation of the average crystallite size of the as-

deposited films has been plotted as a function of Co-content of the films in Figure 4.19. The average crystallite size is found to decrease with Co doping from 18.01 nm for 11 at. % Co to 10.27 nm for Co 28 at. % and then starts increasing to 11.86 nm for 30 at. % Co.

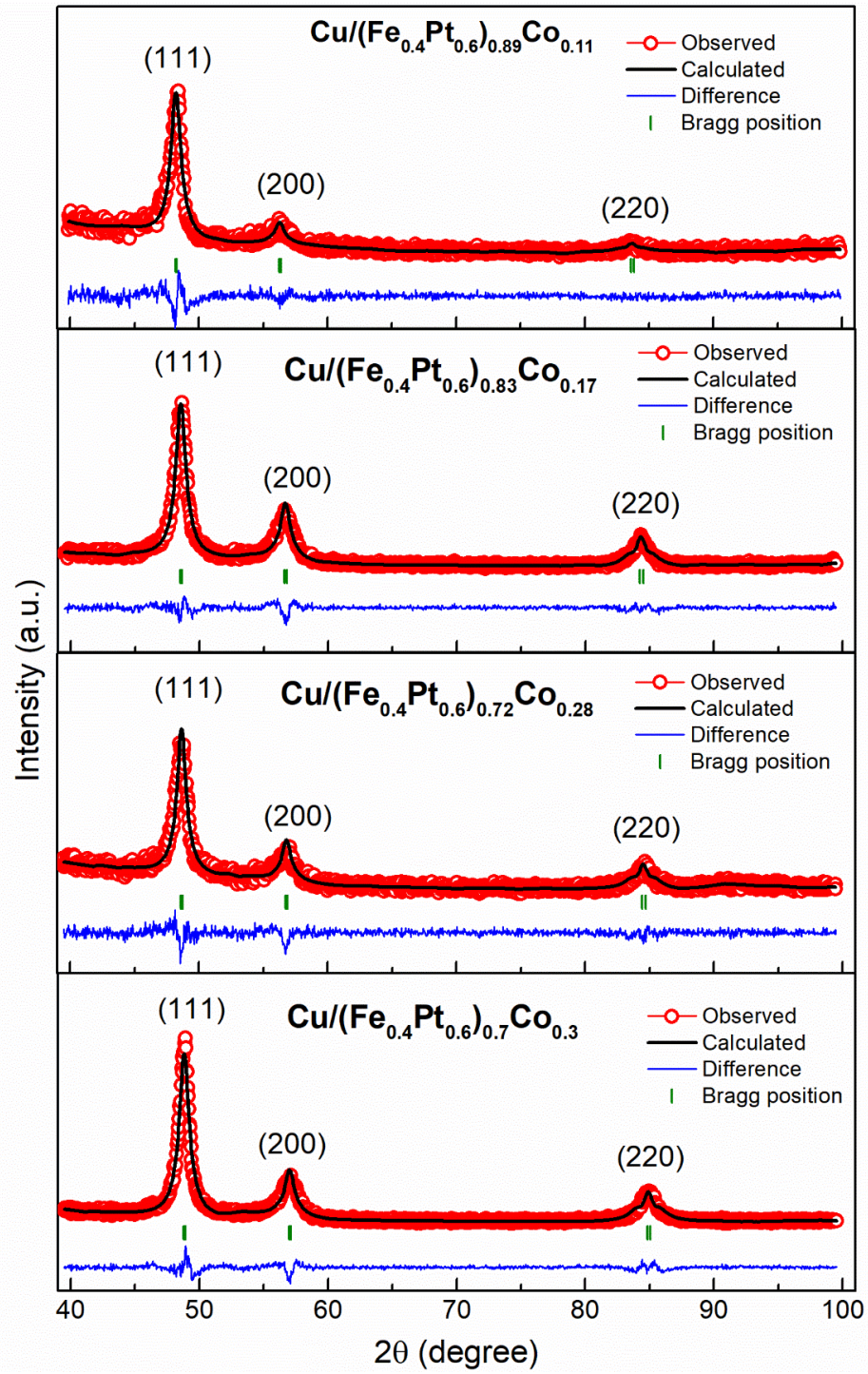

Figure 4.18 Room temperature XRD profile along with Rietveld refinement fit of Cu-underlayered FePtCo thin films.

Table 4.8 Lattice parameters obtained from Rietveld refinement and goodness of fit (χ^2), and average crystallite size of Cu-underlayered FePtCo films.

Sample	$(Fe_{0.4}Pt_{0.6})_{1-x}Co_x$	x=0.11	x=0.17	x=0.28	x=0.30
Cu-underlayered	Lattice parameters, a=b=c (Å)	3.79	3.77	3.76	3.75
	χ^2	1.48	1.53	1.35	1.83
	Crystallite size (nm)	18.0(1)	11.2(2)	10.2(7)	11.8(6)
	Adj. R^2	0.93	0.99	0.97	0.99

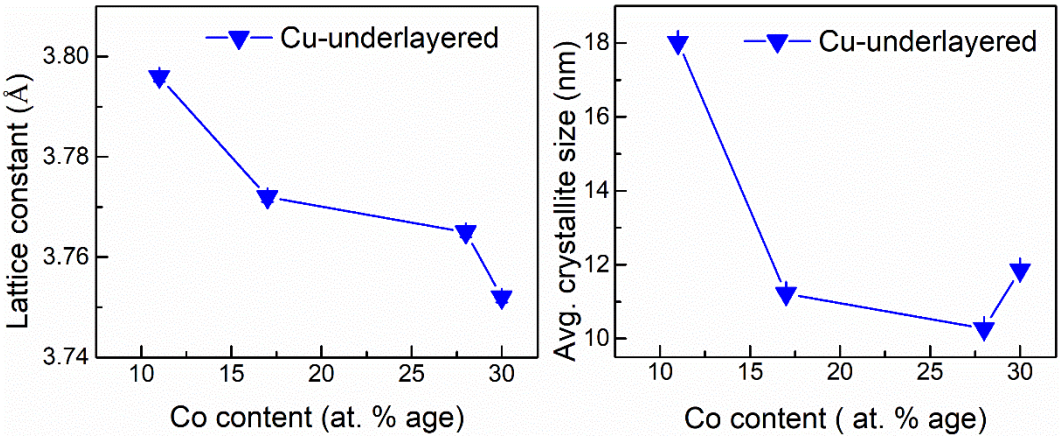

Figure 4.19 Plot of lattice parameter (left) and average crystallite size of Cu-underlayered FePtCo films as a function of Co content of the films.

4.5.4 Influence of Deposition Conditions on XRD Results

From the XRD results of all samples prepared under the three deposition conditions, it is seen that the annealing of the samples at a temperature of 673 K does not transform the crystal structure. This indicates that 673 K is not sufficient to transform the crystal structure of these thin films from chemically disordered FCC structure to chemically ordered $L1_0$ structure. The crystal structure of these films are also not influence by the insertion of 2 nm Cu-under layer to these thin films.

However, the deposition condition do influence the unit cell parameters and the crystallite size. From Figure 4.20 (left) it is clear that the annealing of the films reduces lattice constants except for 11 at. % and 17 at. % Co doped. The FePtCo films with Cu-underlayer are also found to possess smaller lattice parameters than that of corresponding as-deposited thin films. This indicates that insertion of Cu-underlayer also helps in reduction of size of unit cell. The crystallite size on the other hand varies differently for all films deposited under three conditions as evident from Figure 4.20 (right). No particular pattern of variation of crystallite size of same composition prepared at different condition has been observed. This indicates that the crystallite size of these films also depends on other factors along with film composition and film deposition conditions.

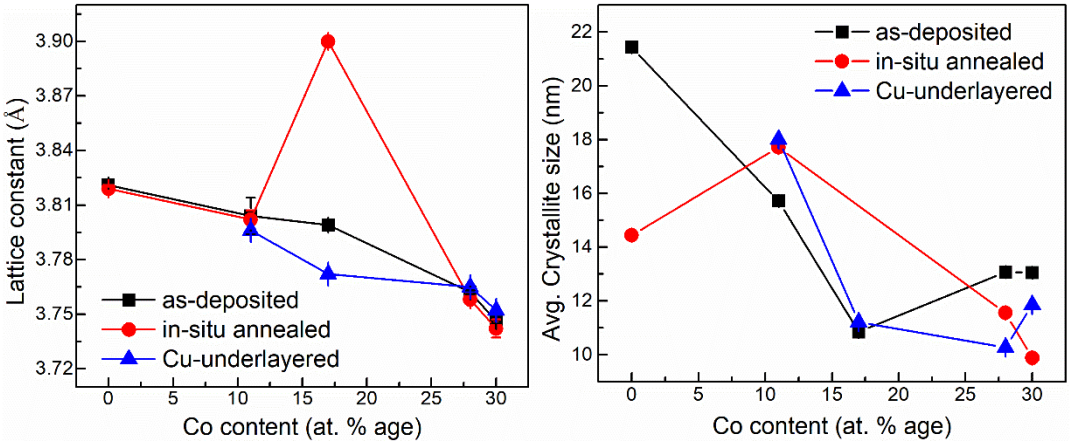

Figure 4.20 Plot of lattice constant (left) and average crystallite size (right) of all FePtCo thin films deposited under three conditions.

4.6 Magnetic Properties of FePtCo Ternary Alloy Thin Film

The magnetic properties of FePtCo ternary alloy thin films prepared under three deposition conditions are characterized by room temperature M-H hysteresis. The measurement were carried out by vibrating sample magnetometer (VSM). To measure the magnetic moment, the samples are cut in pieces of dimension 5 mm× 5 mm. The samples are then attached to the sample holder rod. To take the sample holder rod and substrate contribution to the magnetic moment into account, the magnetic moment of sample holder rod and substrate is first measured in the applied field range of 0 Oe to ±15000 Oe. The total magnetic moment of the films and rod

are then measured at room temperature in the magnetic field range from 0 Oe to ± 15000 Oe. The magnetic moment of sample holder rod is then subtracted from the obtained total magnetic moment to get actual moment of the sample. The magnetic moments are measured in two directions, one by applying magnetic field in the direction parallel to plane of film called in-plane magnetization and the other by applying magnetic field in the direction perpendicular to the plane of film called out-of-plane magnetization. The magnetic moment per unit volume i.e., magnetization of all samples are then calculated by dividing the obtained magnetic moment by volume of the thin film and the magnetization is expressed in emu/cc.

4.6.1 Room Temperature M-H Measurement Results of As-deposited Thin Films

The room temperature in-plane and out-of-plane M-H hysteresis curves obtained for as-deposited pure $Fe_{40}Pt_{60}$ alloy thin film is depicted in Figure 4.21 and the magnetic parameters obtained after subtracting the Si substrate contribution are presented in Table 4.9. The in-plane M-H curve possesses small coercive field (H_C) of 46 Oe whereas the out-of-plane M-H curve possesses larger coercive field (H_C) of 177 Oe. This indicates that a larger magnetic field is required to magnetize the $Fe_{40}Pt_{60}$ alloy thin film in out-of-plane direction than in-plane direction. Thus this film is magnetically harder in out-of-plane direction. On the other hand, the film has a greater remanent magnetization in in-plane direction than out-of-plane direction. Thus M-H curve of the film possesses better squareness of 0.70 in-plane direction than the squareness of 0.08 in out-of-plane M-H curve which can be clearly seen in the inset of Figure 4.21. From Figure 4.21 it has also been observed that the in-plane magnetization saturates at 2100 emu/cc at a much lower applied field than that of out-of-plane magnetization. This shows that the film can be magnetized much easier in in-plane direction than in out-of-plane direction. Thus the $Fe_{40}Pt_{60}$ alloy film exhibits in-plane magnetic anisotropy with an easy axis along direction of film plane. Such in-plane magnetic anisotropic behavior is generally observed in other chemically disordered FCC structured FePt-based alloy thin films [85]. The effective anisotropic constant (K_{eff}) of the film is calculated by finding the area difference enclosed by the in-plane and out-of-plane M-H

curves [11,30–32,80]. To calculate the effective anisotropic constant, only the initial magnetization of both in-plane and out-of-plane M-H loops is considered. Then the difference in area enclosed by the in-plane and out-of-plane magnetization curves is found by integrating the initial magnetization curves and x-axis using Originlab software. This area difference enclosed by the two initial magnetization curves is the indicative value of effective anisotropic constant. The integrated M-H curves are presented in Figure 4.22 and the obtained value of K_{eff} is presented in Table 4.9. The obtained value of K_{eff} indicates that the film exhibit a very large effective anisotropic energy of 2.09×10^{7} erg/cc.

Table 4.9 Coercivity, saturation magnetization, remanent magnetization, squareness of room temperature in-plane and out-of-plane M-H hysteresis curve and effective anisotropic constant (K_{eff}) of as-deposited FePt alloy film obtained after correction of substrate contribution.

Sample	Direction	H_C (Oe)	M_S (emu/cc)	M_r (emu/cc)	M_r/M_S	K_{eff} (erg/cc)
$Fe_{40}Pt_{60}$	In-plane	46	2100	1467	0.70	2.09×10^7
	Out-of-plane	177		161	0.08	

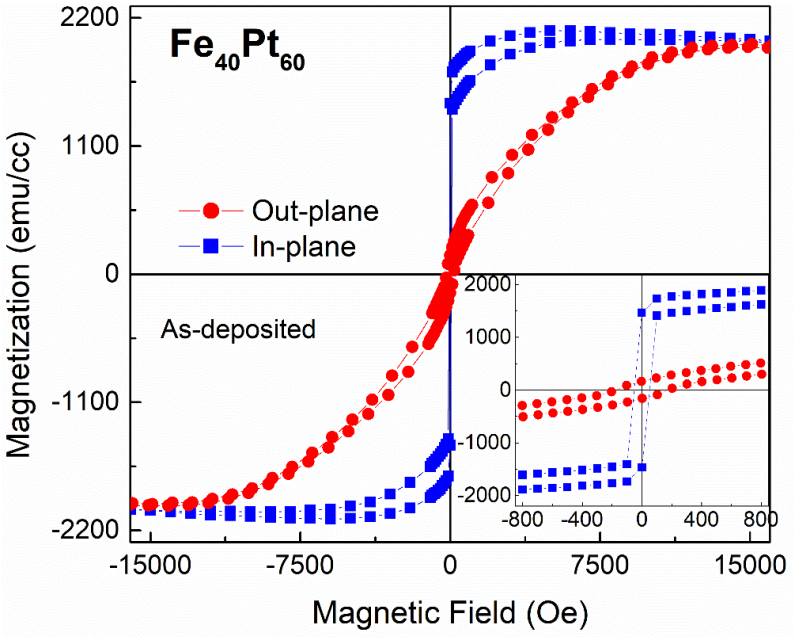

Figure 4.21 Room temperature M-H hysteresis curve of as-deposited pure FePt alloy thin film.

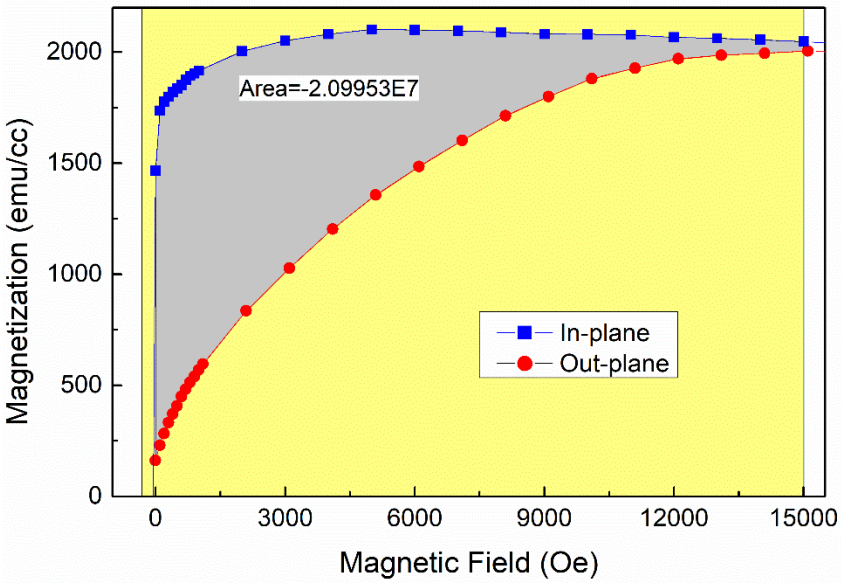

Figure 4.22 Calculation of area difference enclosed by in-plane and out-of-plane initial magnetization curves of $Fe_{40}Pt_{60}$ alloy thin film.

Figure 4.23 presents the room temperature in-plane and out-of-plane M-H hysteresis curves obtained for 11 at. % Co-doped as-deposited FePtCo alloy thin film. The room temperature magnetic parameters such as H_C, M_S, M_r, and M_r/M_S for 11 at. % Co-doped film obtained after correction of substrate contribution to M-H data are presented in Table 4.10. The film has a small in-plane H_C of 63 Oe whereas it has a larger out-of-plane H_C of 237 Oe indicating that the film is magnetically harder in out-of-plane direction. The in-plane M-H curve saturates at 1702 emu/cc with remanent magnetization of 1340 emu/cc. Thus in-plane M-H curve is nearly square hysteresis with a squareness value of 0.79. On the other hand, the out-of-plane M-H loop has much smaller remanence of 66 emu/cc and possesses a small squareness value of 0.04. From Figure 4.23 it is also observed that in-plane M-H curve saturates at a much lower applied field than out-of-plane M-H curve. Thus 11 at. % Co-doped FePtCo thin film also exhibits in-plane magnetic anisotropy with an easy axis along parallel to plane of film. The effective anisotropic energy is calculated from M-H curve in similar way as stated above for pure FePt film using Originlab software. The calculation is presented in Figure 4.24 and the obtained value of K_{eff} is listed in Table 4.10. The K_{eff} value of 11 % Co doped film is found to be 9.76×10^6 erg/cc which is smaller than the K_{eff} of pure FePt film.

Table 4.10 Coercivity, saturation magnetization, remanent magnetization, squareness of room temperature in-plane and out-of-plane M-H hysteresis curve and K_{eff} of as-deposited $(Fe_{0.4}Pt_{0.6})_{0.89}Co_{0.11}$ alloy film obtained after correction of substrate contribution.

Sample	Direction	H_C (Oe)	M_S (emu/cc)	M_r (emu/cc)	M_r/M_S	K_{eff} (erg/cc)
$(Fe_{0.4}Pt_{0.6})_{0.89}Co_{0.11}$	In-plane	63	1702	1340	0.79	9.76×10^6
	Out-of-plane	237		66	0.04	

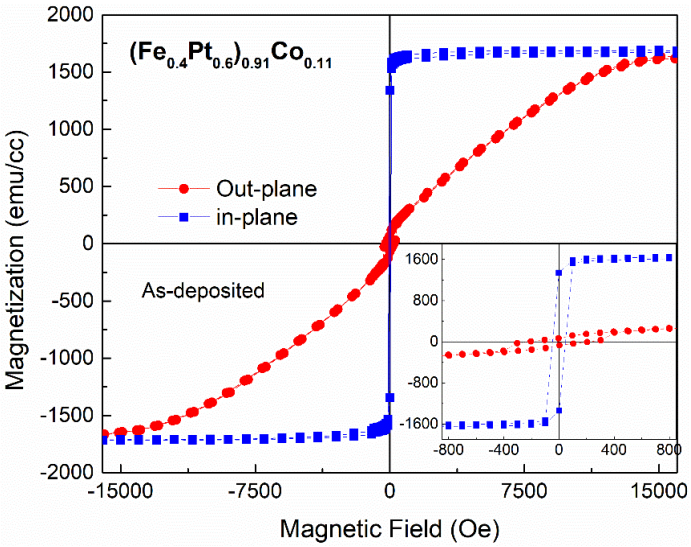

Figure 4.23 Room temperature M-H hysteresis curve of as-deposited 11 at. % Co doped FePt alloy thin film.

Figure 4.25 shows the room temperature M-H hysteresis loop of 17 at. % Co-doped film and magnetic parameters obtained are presented in Table 4.11. The data have been presented after correction of M-H contribution from substrate. The 17 at. % Co doped film possesses smaller in-plane coercivity of 53 Oe than out-of-plane H_C of 91 Oe indicating that the film is also magnetically harder in out-of-plane direction. This film also possesses a very large remanent magnetization of 1569 emu/cc in in-plane as compared to the remanence of 19 emu/cc in out-of-plane direction. Thus the film exhibit a nearly square in-plane M-H loop with squareness

value of 0.86 and much smaller squareness of 0.01 of out-of-plane M-H loop. The in-plane M-H loop is also found to saturate at 1824 emu/cc at much lower field than the out-of-plane M-H loop as evident from Figure 4.25. This shows that this film also exhibits in-plane magnetic anisotropy with an easy axis parallel to plane of film. The effective anisotropic constant K_{eff} of the film is also calculated by calculating the area difference enclosed by the in-plane and out-of-plane M-H curves. The calculated area difference is indicated by the shaded region with light gray colour in Figure 4.26 and found to be 1.10×10^{7} erg/cc which is the indicative value of in-plane K_{eff} of this film.

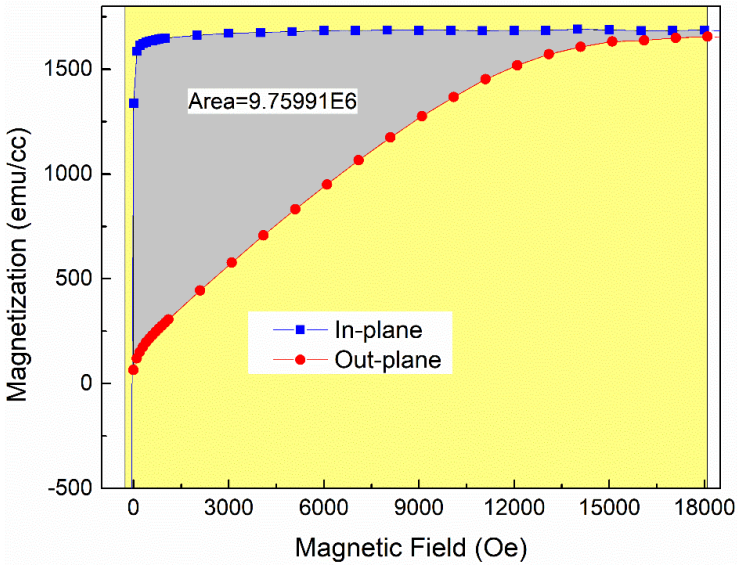

Figure 4.24 Calculation of area difference enclosed by in-plane and out-of-plane initial magnetization curves of $(Fe_{0.4}Pt_{0.6})_{0.89}Co_{0.11}$ alloy thin film.

Table 4.11 Coercivity, saturation magnetization, remanent magnetization, squareness of room temperature in-plane and out-of-plane M-H hysteresis curve and K_{eff} of as-deposited $(Fe_{0.4}Pt_{0.6})_{0.83}Co_{0.17}$ alloy film obtained after substrate correction.

Sample	Direction	H_C (Oe)	M_S (emu/cc)	M_r (emu/cc)	M_r/M_S	K_{eff} (erg/cc)
$(Fe_{0.4}Pt_{0.6})_{0.83}Co_{0.17}$	In-plane	53	1824	1569	0.86	1.10×10^{7}
	Out-of-plane	91		19	0.01	

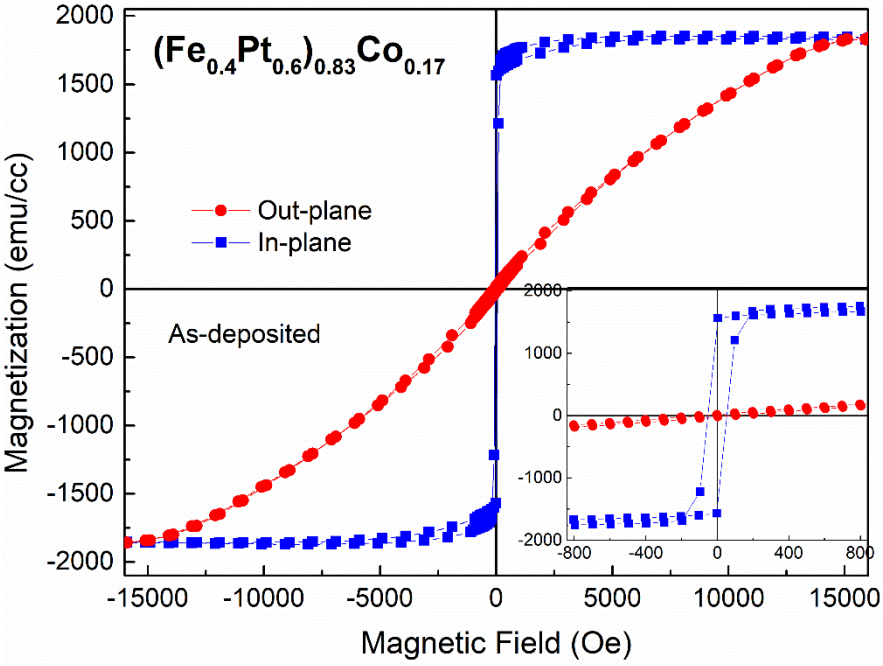

Figure 4.25 Room temperature M-H hysteresis curve of as-deposited 17 at. % Co doped FePt alloy thin film.

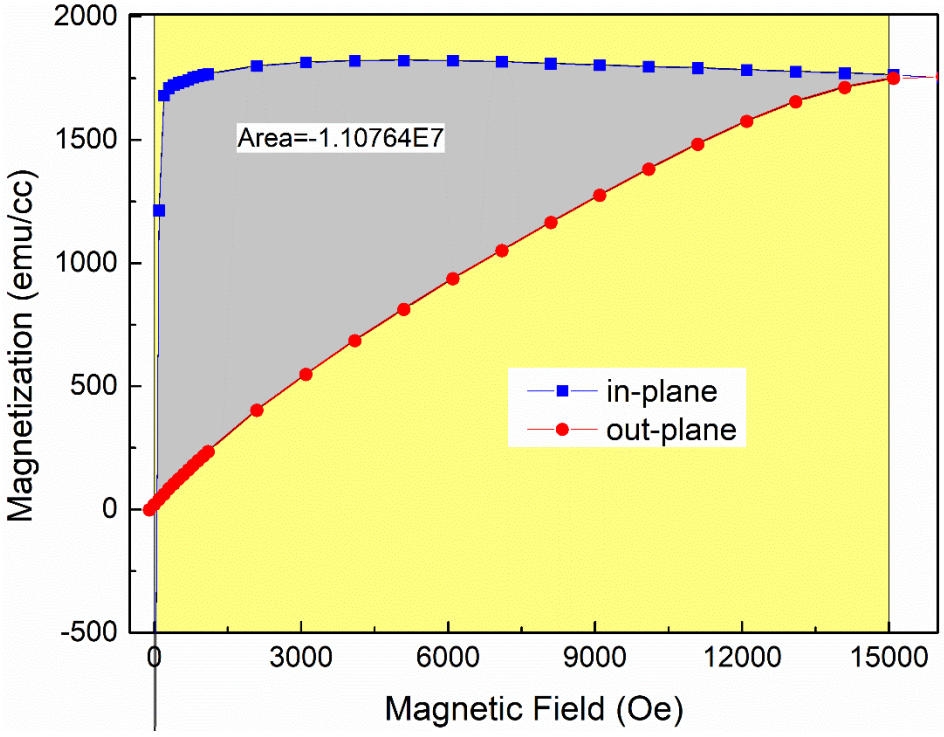

Figure 4.26 Calculation of area difference enclosed by in-plane and out-of-plane initial magnetization curves of $(Fe_{0.4}Pt_{0.6})_{0.83}Co_{0.17}$ alloy thin film.

The 28 at. % Co doped film exhibit nearly the same in-plane H_C (78 Oe) and out-of-plane H_C (82 Oe) as seen in Table 4.12 which can also be clearly seen in the inset of Figure 4.27. The in-plane M-H curve also possesses large remanence of 1300 emu/cc with saturation magnetization 1479 emu/cc thus possessing large squareness value of 0.88. On the other hand the out-of-plane magnetization has very small remanent magnetization of 30 emu/cc and possesses very small squareness value of 0.02. The in-plane M-H loop is also seen to be saturate at a much smaller applied magnetic field than the out-of-plane M-H loop producing a large difference in area enclosed by the M-H loop in two directions as seen in Figure 4.27. This indicates that the 28 at. % Co doped film is also magnetized in in-plane direction with much smaller field than in out-of-plane direction. Thus this film also exhibits in-plane magnetic anisotropy with easy axis along the plane of film and the hard axis in perpendicular the plane of film. The calculation of effective anisotropy energy from the area enclosed by in-plane and out-of-plane M-H loops (Figure 4.28) gives the K_{eff} value of 7.34×10^6 erg/cc. The magnetic parameters such as M_S, H_C, M_r, squareness and K_{eff} obtained for 28 at. % Co doped FePt film are presented in Table 4.12. The data have been presented after correction of M-H contribution from substrate.

Table 4.12 Coercivity, saturation magnetization, remanent magnetization, squareness of room temperature in-plane and out-of-plane M-H hysteresis curve and effective anisotropic constant (K_{eff}) of as-deposited $(Fe_{0.4}Pt_{0.6})_{0.72}Co_{0.28}$ alloy film obtained after substrate correction.

Sample	Direction	H_C (Oe)	M_S (emu/cc)	M_r (emu/cc)	M_r/M_S	K_{eff} (erg/cc)
$(Fe_{0.4}Pt_{0.6})_{0.72}Co_{0.28}$	In-plane	78	1479	1300	0.88	7.34×10^6
	Out-of-plane	82		30	0.02	

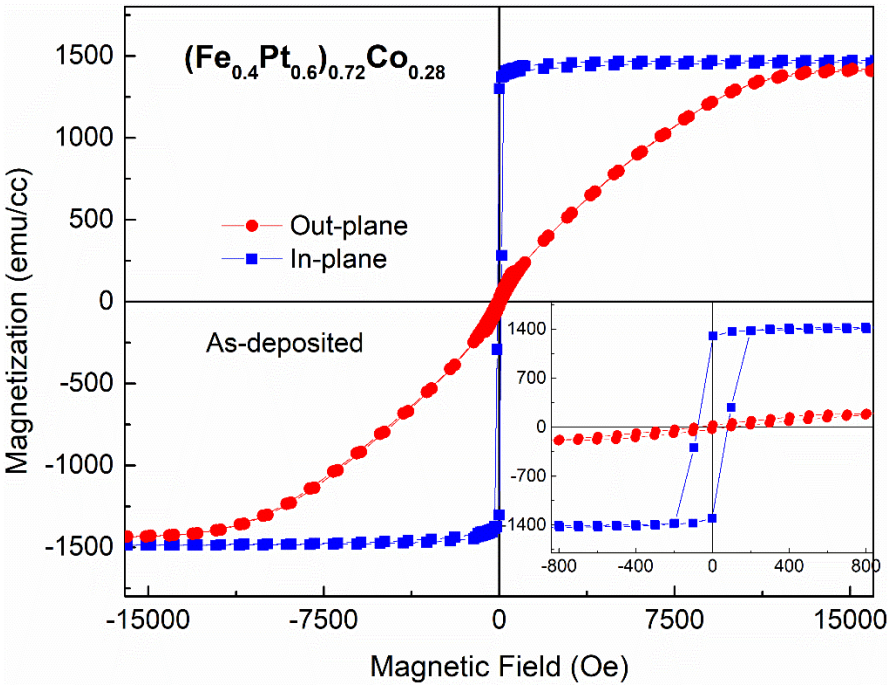

Figure 4.27 Room temperature M-H hysteresis curve of as-deposited 28 at. % Co doped FePtCo alloy thin film.

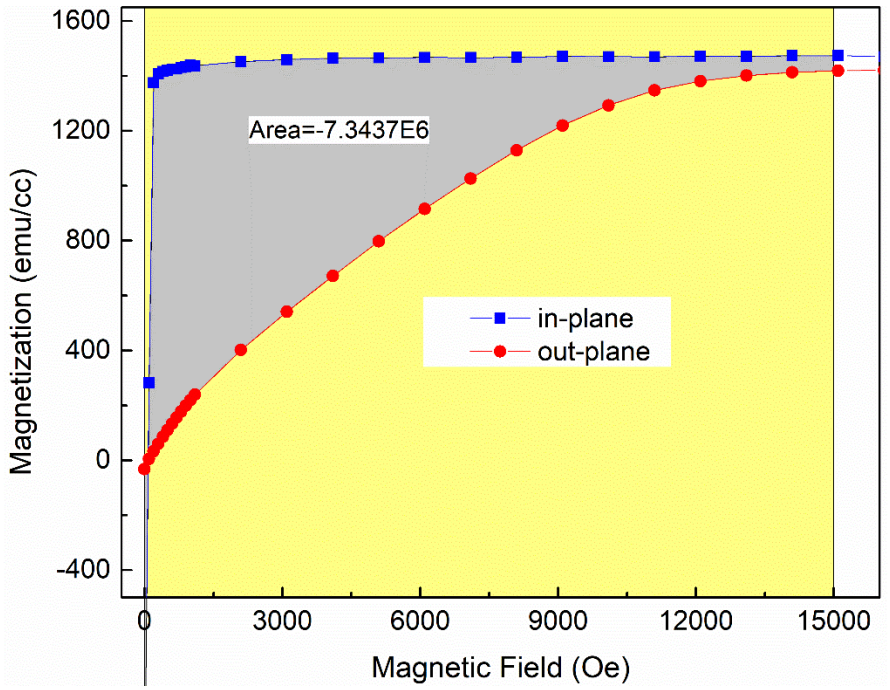

Figure 4.28 Calculation of area difference enclosed by in-plane and out-of-plane initial magnetization curves of $(Fe_{0.4}Pt_{0.6})_{0.72}Co_{0.28}$ alloy thin film.

The room temperature M-H hysteresis loop for 30 at. % Co-doped film is presented in Figure 4.29 and the obtained magnetic parameters after correction of substrate contribution are illustrated in Table 4.13. It is observed that this film exhibit a larger coercivity of 72 Oe in in-plane direction than the coercivity of 31 Oe in perpendicular direction. This indicates that the film is magnetically harder in in-plane direction. However, the in-plane magnetization saturates at 1326 emu/cc at much smaller applied than out-of-plane magnetization. This indicates that this film also exhibit in-plane magnetization with easy axis along plane of film and the hard axis in perpendicular to the film plane. The effective anisotropic constant calculation from the area enclosed by in-plane and out-of-plane M-H curves (Figure 4.30) gives the value of 6.57×10^{6} erg/cc. The in-plane M-H curve has also a large remanent magnetization of 1166 emu/cc, thus possessing nearly square hysteresis loop with squareness value of 0.88. On the other hand, the out-of-plane M-H curve has a very small remanent magnetization of 16 emu/cc and squarness value of 0.01 which is indeed much smaller than that obtained for in-plane magnetization.

Table 4.13 Coercivity (H_C), saturation magnetization (M_S), remanent magnetization (M_r), squareness (M_r/M_S) of room temperature in-plane and out-of-plane M-H hysteresis curve and effective anisotropic constant (K_{eff}) of as-deposited $(Fe_{0.4}Pt_{0.6})_{0.70}Co_{0.30}$ alloy film obtained after substrate correction.

Sample	Direction	H_C (Oe)	M_S (emu/cc)	M_r (emu/cc)	M_r/M_S	K_{eff} (erg/cc)
$(Fe_{0.4}Pt_{0.6})_{0.70}Co_{0.30}$	In-plane	72	1326	1166	0.88	6.57×10^{6}
	Out-of-plane	31		16	0.01	

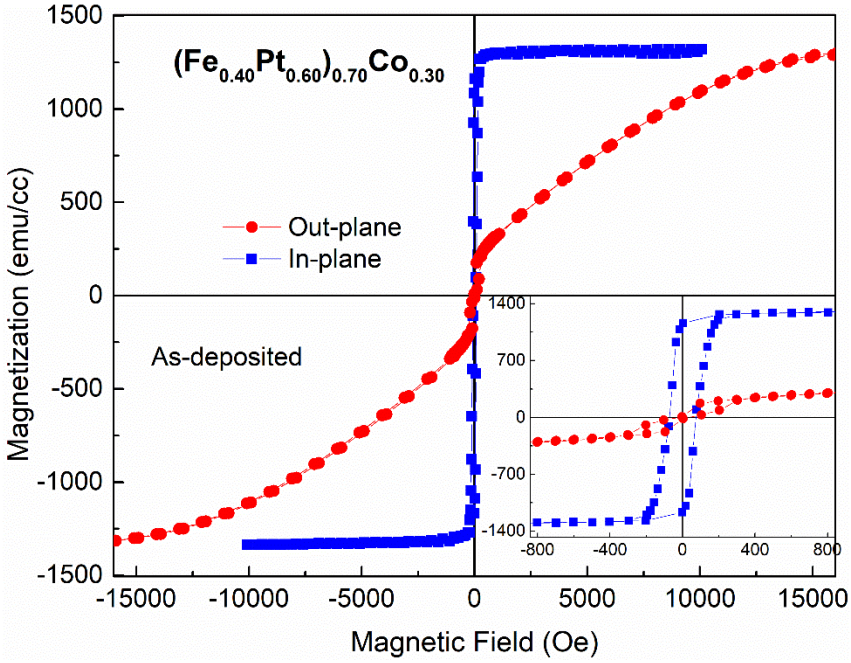

Figure 4.29 Room temperature M-H hysteresis curve of as-deposited 30 at. % Co doped FePt alloy thin film.

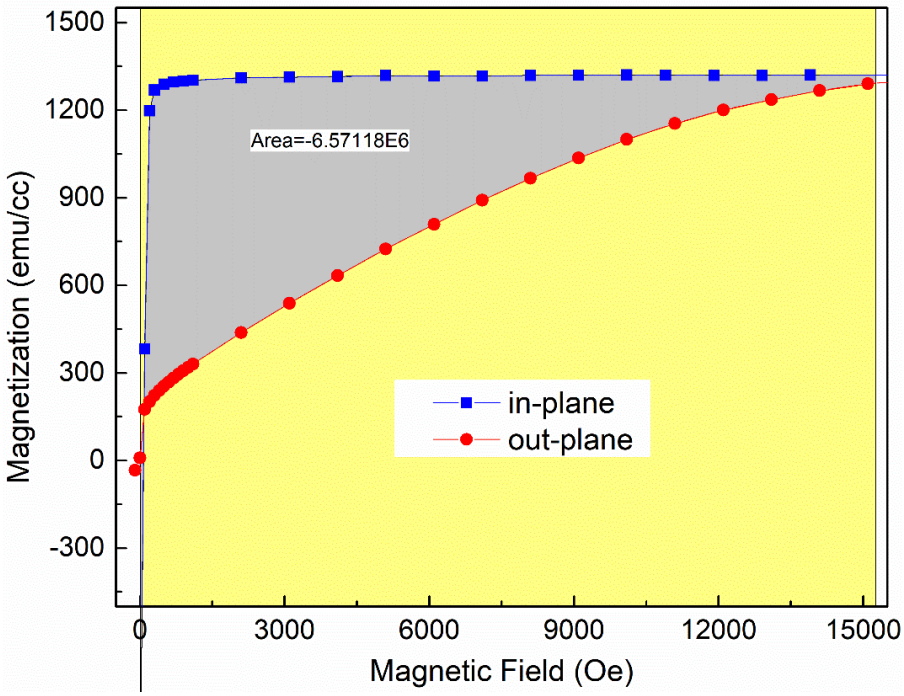

Figure 4.30 Calculation of area difference enclosed by in-plane and out-of-plane initial magnetization curves of as-deposited $(Fe_{0.4}Pt_{0.6})_{0.70}Co_{0.30}$ alloy thin film.

The variation of H_C, M_S, squareness and K_{eff} obtained after correction of substrate contribution of all as-deposited films as a function of Co content (at. % age) have

been plotted in Figure 4.31. The inset of the figures represent the plot of M_S, squareness and K_{eff} as a function of Co content without substrate correction. From Figure 4.31(a), it is seen that the coercivity in-plane magnetization of as-deposited films gradually increases with an increase in Co content of the films and varies in the range of 46 Oe to 76 Oe. On the other hand, the coercivity of out-of-plane magnetization is found to first increase from 177 Oe for pure FePt film to 237 Oe for 11 at. % Co doped film. On further increase of Co content, the out-of-plane coercivity decreases to 31 Oe for 30 at. % Co doped film. Thus out-of-plane H_C shows overall decreasing trend with increase in Co content as shown in Figure 4.31 (a). Also a crossover in variation of in-plane and out-of-plane H_C is observed nearly at 28 at. % Co doping below which these films possess larger H_C in out-plane direction than in-plane and above which out-plane H_C is smaller than in-plane H_C. No difference in in-plane and out-of-plane H_C have been observed before and after subtraction of M-H contribution of substrate. In Figure 4.31 (b) the variation of M_S and M_r as a function of Co content of all the as-deposited films are presented. No appreciable change in M_S and M_r have been noticed after substrate correction except for Co 11 at. %, in which in-plane M_r shows a small decrease due to substrate correction. The M_S decreases from 2100 emu/cc for pure FePt film to 1702 emu/cc on Co doping to 11 at. %. On further increase of Co doping to 17 at. %, small increase in M_S to 1824 emu/cc is observed. Beyond 17 at. % Co doping, The M_S decreases with an increase in Co content and thus overall decreasing trend of M_S with Co doping is seen in Figure 4.31 (b). This observation suggests that the Co doping favours antiferromagnetic interaction with FePt sublattice. The similar results have been reported by a number of researchers in third elements such as Mn [119,136,137,139], Nd [148], Tb [30], Rh [243] etc., doped FePt films. The M_r of in-plane magnetization of these films also shows similar variation as M_S of these films as shown in Figure 4.31(b). As Co doping increases the in-plane M_r vs Co content curve approaches the M_S curve which also indicates the increase in the squareness of in-plane M-H hysteresis loop as shown in Figure 4.31(c). The squareness of in-plane M-H curve of Co 11 at. % is slightly reduced due to substrate correction. However, squareness of in-plane M-H curves show gradual overall increase with increase in Co content of the films. The out-of-plane M-H loop of all

films possesses very small M_r in the range of 16 emu/cc to 161 emu/cc, which decreases with Co doping. Thus a decrease in squareness of the out-of-plane M-H loop is seen (Figure 4.31(c)) with an increase in Co-doping. The variation of K_{eff} as a function of Co content of all as-deposited films is plotted in Figure 4.31 (d). After subtracting the substrate contribution, the value of K_{eff} decreases with Co addition from 2.09×10^7 erg/cc for pure FePt film to 9.76×10^6 erg/cc for 11 at. % Co doped film, then shows a small rise to 1.10×10^7 erg/cc for 17 at. % Co. Further increase of Co addition results a steady fall of K_{eff} up to 6.57×10^6 erg/cc for 30 at. % Co. The nature of variation of K_{eff} is found to be identical to that of M_S of these films. The results indicate that Co addition to FePt alloy results reduction in magnetization and magnetic anisotropy due to antiferromagnetic coupling of Co with FePt.

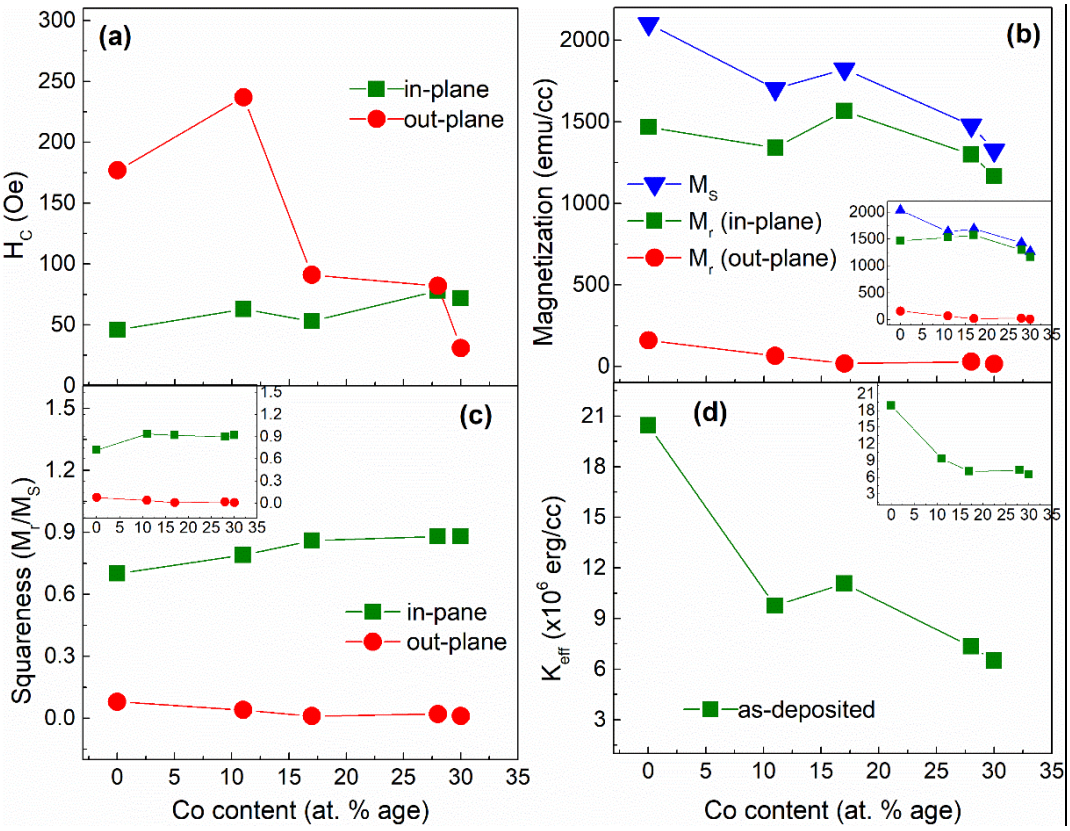

Figure 4.31 Plot of variation of (a) H_C, (b) M_S and M_r, (c) squareness and (d) K_{eff} as a function of Co content of all as-deposited FePtCo alloy thin films. The inset of figure (b), (c) and (d) represents the magnetic parameters obtained from M-H curves without subtracting substrate contribution.

4.6.2 Room Temperature M-H Measurement Results of In-situ Annealed Thin Films

The room temperature M-H hysteresis curves in-situ annealed pure FePt, 11 and 17 at. % Co doped films are presented in Figure 4.32, and obtained magnetic parameters H_C, M_S, M_r and K_{eff} are presented in Table 4.14. All data have been presented after subtracting the substrate contribution and no appreciable increase in magnetic parameters have been noticed. The annealed pure $Fe_{40}Pt_{60}$ alloy film has in-plane H_C of 82 Oe and out-of-plane H_C of 14 Oe indicating that the film is magnetically harder in in-plane direction. The film possesses a large saturation magnetization of 2510 emu/cc. Very large in-plane remanent magnetization of 2413 emu/cc is observed whereas the out-plane remanence of 5 emu/cc is comparatively smaller. Thus the film exhibit a nearly square in-plane M-H hysteresis loop with a squareness value of 0.96 and very small out-of-plane squareness value of 0.002 which can be clearly seen in the inset of Figure 4.32 of pure FePt film. The in-plane magnetization of pure FePt film is found to saturate at much smaller applied field than the out-of-plane magnetization. This indicates that the film can be magnetized with smaller applied field in in-plane direction. Thus this film exhibit in-plane magnetic anisotropy with easy axis along in-plane direction. The effective magnetic anisotropic constant K_{eff} is calculated from M-H curves using the same procedure as stated in the previous section. The calculated area difference is indicated by the shaded region in grey colour in Figure 4.30. The film possesses very large K_{eff} value of 1.31×10^7 erg/cc which is sufficient for application for recording media. The 11 at. % Co doped film on the other hand has a larger out-of-plane H_C of 931 Oe than the in-plane H_C of 72 Oe and M_S of 1780 emu/cc. But in-plane remanent magnetization of 1733 emu/cc is much larger than the out-of-plane remanence 233 emu/cc. This film also exhibits nearly square in-plane M-H loop with squareness value of 0.97 and out-of-plane M-H loop of small squareness value of 0.13 which can also be seen from inset of Figure 4.32 (b). The film also exhibit in-plane magnetic anisotropy with an easy axis parallel to the plane of film which is evident from the in-plane and out-plane M-H curves saturates at different applied fields. The calculation of effective anisotropy energy gives 7.63×10^6 erg/cc. The 17 at.

% Co doped film on the other hand possesses larger in-plane H_C of 86 Oe than out-of-plane H_C of 33 Oe and has smaller saturation magnetization of 495 emu/cc than the pure FePt and 11 at. % Co doped films. The remanence of in-plane and out-of-plane magnetization of the film is found to be 435 and 22 emu/cc respectively with respective corresponding squareness of 0.88 and 0.04. This film also exhibit in-plane magnetic anisotropy with K_{eff} 1.28×10^6 erg/cc which is also smaller than the K_{eff} value of pure FePt and 11 % doped FePtCo film. Figure 4.33 presents the room temperature M-H measurement results of FePtCo films with 28 and 30 at. % Co and the obtained magnetic parameters are presented in Table 4.14. The data have been presented after correction of M-H contribution from substrate. No significant change in magnetic parameters have been observed except a small increase in M_S and K_{eff} after subtracting the Si substrate contribution to M-H curves. The film with 28 at. % Co has an in-plane H_C of 73 Oe which is larger than the out-plane H_C of 47 Oe and M_S of 1204 emu/cc. This film has a large value of in-plane remanent magnetization of 1163 emu/cc and thus possesses nearly square in-plane M-H loop of squareness 0.97. On the other hand, this film possesses a small out-plane remanent magnetization of 118 emu/cc and hence smaller squareness of 0.10. Similar to the pure FePt and other Co doped FeP films, the 28% Co doped film also exhibit in-plane magnetic anisotropy with an easy axis along the plane of film which can be seen in Figure 4.33 (a). The calculation of K_{eff} from M-H loop gives the value of 7.04×10^6 erg/cc. For 30 at. % Co doped film, the observed magnetic characteristic is similar to the film with 11 at. % Co. This film has also a smaller in-plane H_C of 65 Oe than the out-plane H_C of 200 Oe with M_S 1296 emu/cc. The in-plane remanence is found to be 1026 emu/cc thereby giving a squareness value of 0.79 which is relatively smaller than of 11 at. % Co. The out-of-plane remanent magnetization of 90 emu/cc and the corresponding squareness value of 0.07 of this film is also relatively smaller than the film with 11 at. % Co. This film also exhibits in-plane magnetic anisotropy with an easy axis along the plane of film and the calculated value of K_{eff} is found to be 7.45×10^6 erg/cc which is nearly equal to that of film with 11 at. % Co.

The variations of H_C, M_S, M_r, squareness and K_{eff} as a function of Co content of the in-situ annealed FePtCo films are presented in Figure 4.35. The inset of the figures show the variation of M_S, M_r, squareness and K_{eff} without correction of substrate contribution. Referring to Figure 4.35 (a) it is seen that the in-plane coercivity of annealed films gradually decreases with an increase in Co content of films. On the other hand, the out-of-plane coercivity of the films shows an overall increase with Co doping. However, the 11 at. % Co doped film has exceptionally large out-of-plane coercivity the origin of which remains unknown. From Figure 4.35 (b), it is observed that the saturation magnetization decreases with an increase in Co doping up to 17 at. % Co. With further increase in Co doping beyond 17 at. % the saturation magnetization again increases. This variation is identical in nature as the variation of M_S before subtracting the substrate contribution to M-H curves which can be seen in the inset of Figure 4.35 (b). This suggests that there is an optimum value of Co doping in the neighbourhood of 17 at. % up to which Co promotes antiferromagnetic interaction with FePt sublattice. Above the optimum Co doping the ferromagnetic coupling again starts dominating over antiferromagnetic coupling. The in-plane remanent magnetization also varies in a similar manner as saturation magnetization as shown in Figure 4.35 (b). However, a small overall increase in the out-of-plane remanent magnetization is observed. Both in-plane and out-of-plane M_r also show identical variations as a function of Co content of films before substrate contribution to M-H data were corrected as can be seen in inset of Figure 4.35 (b). The in-plane M-H loop of the films shows a small overall decrease in squareness with an increase in Co content of the films. On the other hand, the squareness of out-of-plane M-H loop shows a small increase with increase in Co content as depicted in Figure 4.35 (c). Moreover, the squareness values of out-of-plane M-H loops are much smaller than the squareness of in-plane M-H loop of the respective films due to small remanent magnetization of in out-of-plane direction. These results also indicate the existence of large magnetic anisotropy of these films. As the substrate correction does not result significant change in M_S and M_r of M-H, both in-plane and out-of-plane M-H curves without substrate correction have nearly equal squareness values as that obtained after removing the M-H contribution of substrate. The variation of squareness as a function of Co content is also identical

in nature before and after the substrate correction as it can be seen in the inset of Figure 4.35 (c).

Table 4.14 Coercivity (H_C), saturation magnetization (M_S), remanent magnetization (M_r), squareness (M_r/M_S) of room temperature in-plane and out-of-plane M-H hysteresis curves and effective anisotropic constant (K_{eff}) of all in-situ annealed FePtCo alloy films obtained after subtracting the substrate contribution.

Sample	Direction	H_C (Oe)	M_S (emu/cc)	M_r (emu/cc)	Squareness (M_r/M_S)	K_{eff} (erg/cc)
$Fe_{40}Pt_{60}$	In-plane	82	2510	2413	0.96	1.31×10^7
	Out-of-plane	14		5	0.002	
$(Fe_{0.4}Pt_{0.6})_{0.89}Co_{0.11}$	In-plane	72	1780	1733	0.97	7.63×10^6
	Out-of-plane	931		233	0.13	
$(Fe_{0.4}Pt_{0.6})_{0.83}Co_{0.17}$	In-plane	86	495	435	0.88	1.28×10^6
	Out-of-plane	33		22	0.04	
$(Fe_{0.4}Pt_{0.6})_{0.72}Co_{0.28}$	In-plane	73	1204	1163	0.97	7.04×10^6
	Out-of-plane	47		118	0.10	
$(Fe_{0.4}Pt_{0.6})_{0.70}Co_{0.30}$	In-plane	65	1296	1026	0.79	7.45×10^6
	Out-of-plane	200		90	0.07	

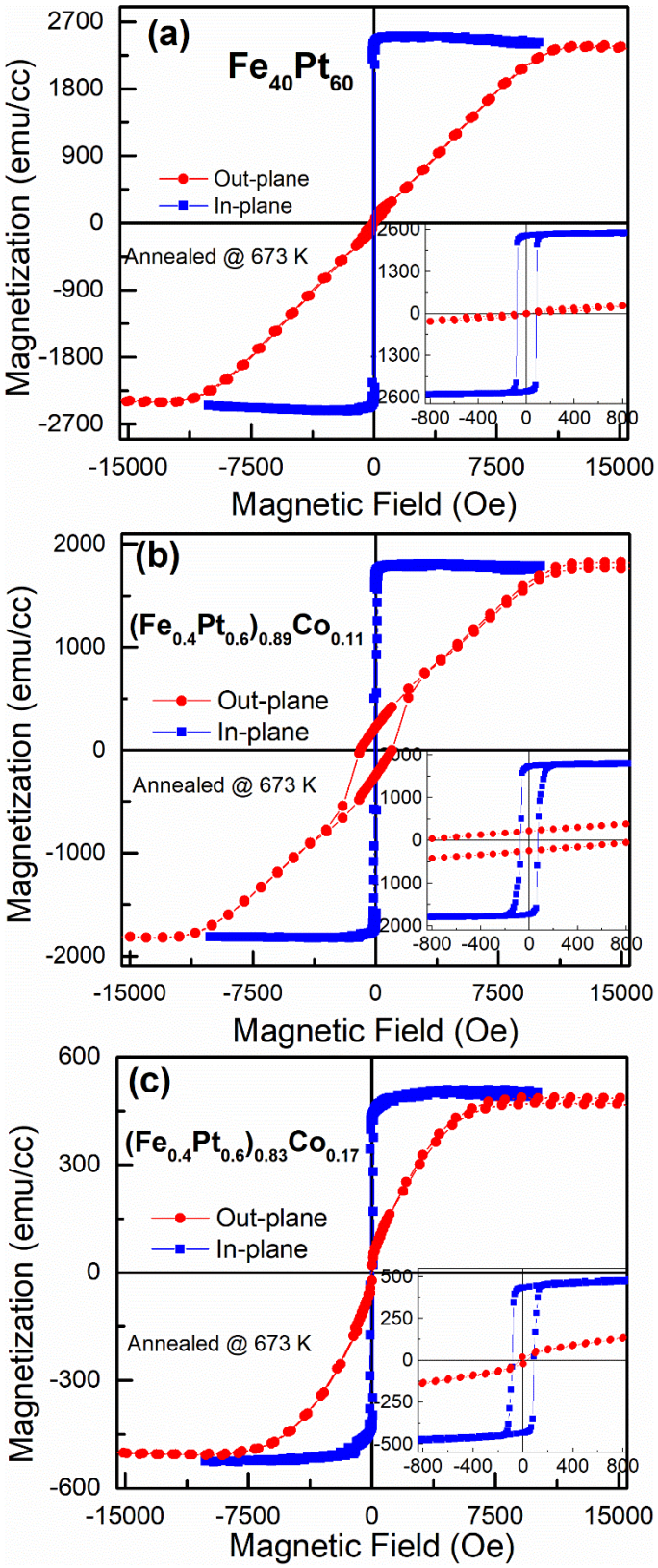

Figure 4.32 Room temperature M-H hysteresis curves of (a) pure FePt, (b) 11 at. % and (c) 17 at. % Co doped in-situ annealed FePtCo films.

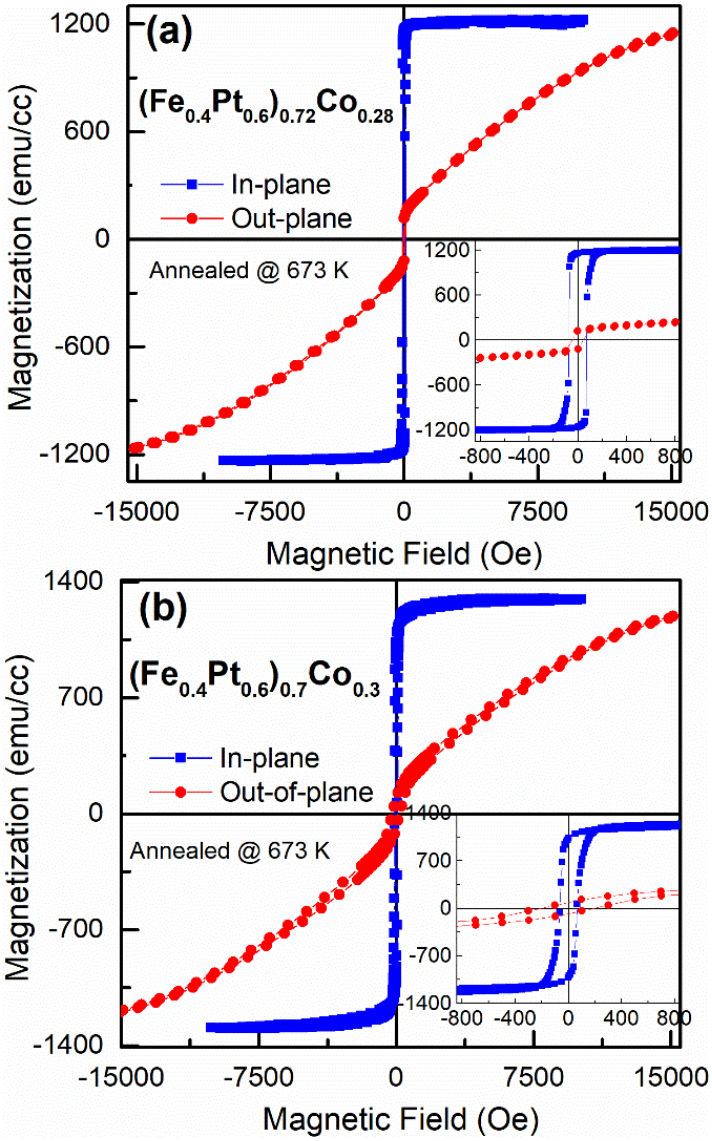

Figure 4.33 Room temperature M-H hysteresis curves of (a) 28 and (b) 30 at. % Co doped in-situ annealed FePtCo films.

The effective magnetic anisotropic energy before (inset of Figure 4.35 (d)) and after (Figure 4.35 (d)) correction of Si substrate contribution to M-H, varies identically which is also similar to the variation of saturation magnetization. The K_{eff} initially decreases with an increase in Co content up to 17 at. % Co. On further increase in Co doping beyond 17 at. % the K_{eff} also increases. This shows that the antiferromagnetic interaction between Co sublattice and FePt sublattice results in a reduction of anisotropy energy. This observation leads to an important inference that by enhancing the ferromagnetic interaction between the host and the dopant, the anisotropy energy can be enhanced.

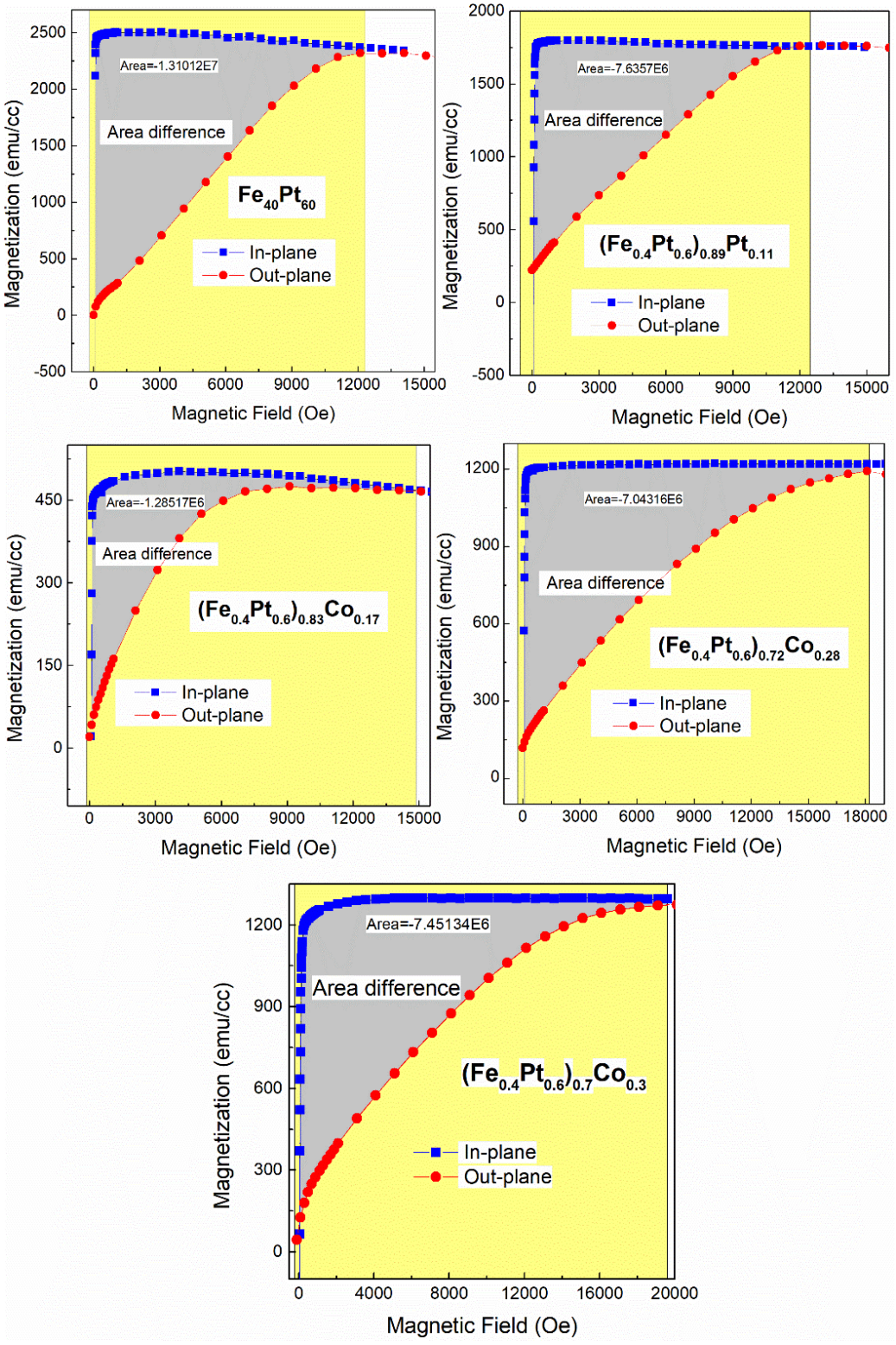

Figure 4.34 Calculation of difference in area enclosed by in-plane and out-plane M-H hysteresis loop of in-situ annealed thin films by integration. The shaded area in grey colour represents the difference in area which is the quantitative value of K_{eff}.

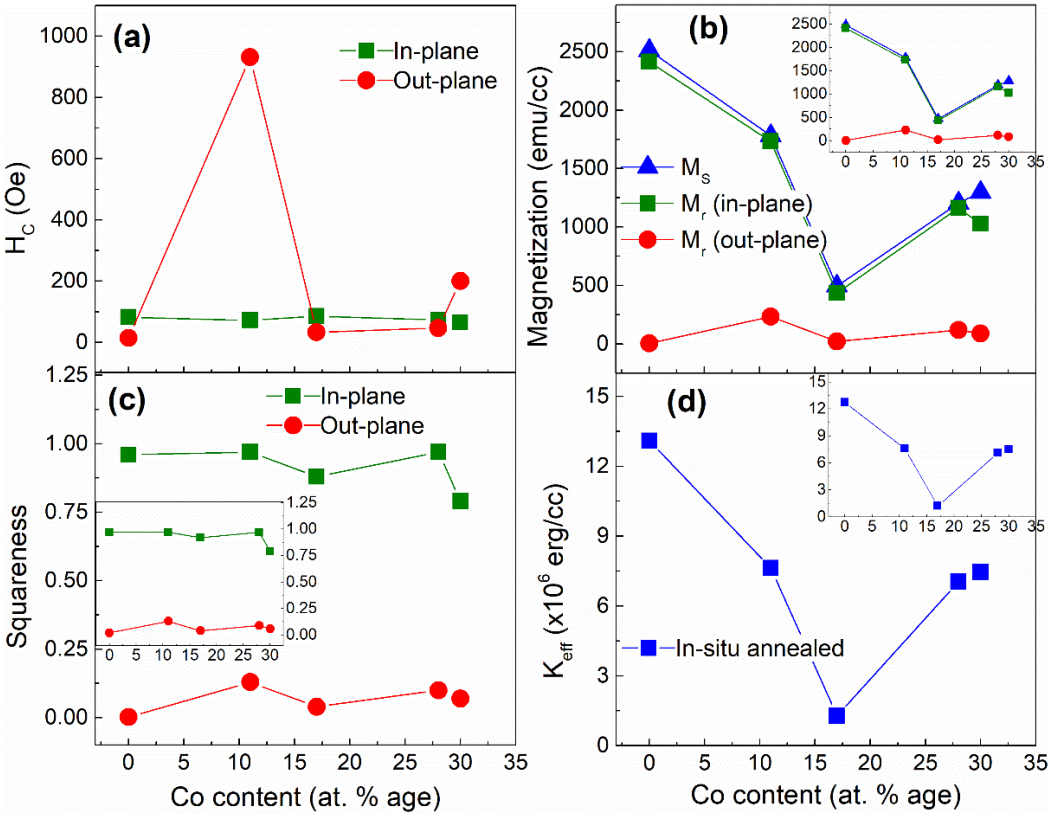

Figure 4.35 Plot of variation of (a) coercivity, (b) Magnetization, (c) squareness and (d) K_{eff} as a function of Co content of in-situ annealed FePtCo films. The inset of figure (b), (c) and (d) represents the magnetic parameters obtained from M-H curves without subtracting substrate contribution.

4.6.3 Room Temperature M-H Measurement Results of Cu-underlayered FePtCo Thin Films

The magnetization (M) measurement results as a function of applied magnetic field (H) at room temperature of all Co-doped Cu-underlayered FePtCo films are presented in Figure 4.36 and Figure 4.37 and obtained magnetic parameters such as H_C, M_S, M_r, squareness (M_r/M_S) and K_{eff} are presented in Table 4.15. Data have been presented after removing M-H contribution of Si substrate. No appreciable increase in M_S, M_r, squareness and K_{eff} is found after subtracting the substrate contribution. The 11 at. % Co doped film is found to possess a smaller in-plane H_C of 73 Oe as compared to the out-plane H_C of 132 Oe indicating that the film is magnetically harder in out-plane direction. The film is found to have a large saturation magnetization of 2291 emu/cc. The in-plane magnetization curve has

large remanence of 2195 emu/cc thus exhibiting a nearly square hysteresis loop of squareness value of 0.96. On the other hand, the out-of-plane magnetization possesses smaller remanent magnetization of 289 emu/cc with a squareness value of 0.13. From Figure 4.36 (a) it is seen that the in-plane magnetization saturates at a much smaller applied field as compared to the out-plane magnetization of the film showing different magnetizations in two different directions. The film being magnetized smaller field in in-plane direction than that of out-plane direction, and the magnetic easy axis lies along the in-plane direction. Thus the film exhibits in-plane magnetic anisotropy with magnetic easy axis along the in-plane direction. The effective anisotropy constant K_{eff} is calculated from M-H curve using the same method as detailed in the previous section 4.2.1. The calculation of difference in the area enclosed by in-plane and out-plane M-H curves is presented in Figure 4.38. The shaded region in grey colour represents the difference in area enclosed by in-plane and out-plane M-H curves which is the indicative value of K_{eff}. A large K_{eff} value of 1.32×10^7 erg/cc has been obtained for this film indicating that the film is highly anisotropic. The 17 at. % Co doped film also possesses smaller H_C of 86 Oe in in-plane direction than H_C of 276 Oe in out-plane direction as can be clearly seen in the inset of Figure 4.36 (b). This film has a relatively smaller M_S of 1050 emu/cc than the film with 11 at. % Co. The film also possesses relatively small remanent magnetization in both in-plane (M_r=447 emu/cc) and out-plane (M_r=141 emu/cc) directions, thereby exhibiting in-plane and out-plane M-H hysteresis loop of small squareness of 0.43 and 0.13 respectively as shown in the inset of Figure 4.36 (b). As seen in Figure 4.36, the in-plane magnetization has a lower saturation field than the out-of-plane magnetization indicating that this film also exhibits in-plane magnetic anisotropy with an easy axis along the plane of film. The calculation of anisotropy energy K_{eff} (Figure 4.38) from M-H curves gives the value 2.60×10^6 erg/cc which is smaller than the film with lower Co content of 11 at. %. The room temperature M-H measurement results for other two Cu-underlayered films with 28 at. % and 30 at. % Co are presented in Figure 4.37 and the obtained magnetic parameters are presented in Table 4.15. The data have been presented after correction of M-H contribution from substrate. The film with 28 at. % Co possesses a smaller in-plane H_C of 73 Oe than the out-plane H_C of 115 Oe which is

clearly seen in inset of Figure 4.37 (a) and moderate M_S of 1673 emu/cc. This film possesses a comparatively large in-plane M_r value of 1579 emu/cc which gives large squareness of M-H hysteresis loop of value 0.96. On the other hand, this film possesses a comparatively smaller out-of-plane M_r value of 144 Oe thereby giving a relatively small squareness M-H loop of value 0.09. From Figure 4.37 (a), it is evident that this film also has a smaller saturation field in the in-plane direction as compared to the out-plane magnetization which shows that the film has magnetization easy axis in the direction parallel to the plane of film and hard axis in the perpendicular direction. Thus the film exhibits in-plane magnetic anisotropy with an easy axis parallel to the plane of film. The calculation of K_{eff} (Figure 4.38) gives large value 9.10×10^6 erg/cc which signifies that the film is highly anisotropic. A similar magnetic characteristic is observed for 30 at. % Co doped film showing smaller in-plane H_C (=70 Oe) than the out-plane H_C (=225 Oe) with M_S of 1505. This film with 30 at. % Co also has a sufficiently large in-plane M_r value of 1367 emu/cc and a relatively smaller out-plane M_r of 186 emu/cc as shown in the inset of Figure 4.37 (b). These observed values of M_r give large in-plane squarness of value 0.91 and a relatively smaller out-plane squareness of 0.12. This film also exhibit in-plane magnetic anisotropy with easy axis parallel to film plane and hard axis in perpendicular direction as evident form the Figure 4.37 (b). This film is also found to be highly magnetically anisotropic with large anisotropy energy $K_{eff}=8.17 \times 10^6$ erg/cc.

The variation of magnetic parameters such as H_C, M_S, M_r, squareness (M_r/M_S) and K_{eff} of all Cu-underlayered films are plotted as a function of Co content of the films in Figure 4.39. The inset of Figure 4.39 is plot of M_S, M_r, squareness and K_{eff} as a function of Co content of the films before correction of M-H contribution from substrate. It is seen in Figure 4.39 (a) that the in-plane coercivity first increases with Co content up to 17 at. %. On further increase of Co doping beyond 17 at. %, the in-plane H_C is seen to decrease with an increase Co content of the films. But the variation in H_C is relatively small and lies in the range of 86 Oe to 70 Oe. However, no systematic pattern of variation of out-plane H_C as a function of Co content is observed for these films. Though it can be resembled with letter 'N' like variation, it appears to be difficult to draw an inference from this variation of out-plane H_C.

As shown in Figure 4.39 (b), the M_S sharply decreases with increases in Co doping from 11 to 17 at. %. On further increase in Co doping beyond 17 at. %, an overall increase in M_S is observed. From inset of Figure 4.39 (b) identical nature of variation of M_S before and after the M-H contribution of substrate. This result suggests that the Co doping favours antiferromagnetic interaction between Co sublattice and FePt sublattice up to certain percentage of Co. On further increase of Co doping, again ferromagnetic interaction between the two sublattices dominates over antiferromagnetic interaction due to which rise in M_S has been observed. The in-plane M_r of the films also shows similar variation with Co content as that of M_S and is found to be much larger than the out-plane M_r as depicted in Figure 4.39 (b). The out-plane M_r varies within a small range from 288 to 141 emu/cc. It decreases initially with Co content up to 17 at. % and thereafter shows an increasing trend with increase in Co content. From inset of Figure 4.39 (b), it can be seen that the variation of in-plane and out-of-plane M_r as a function of Co content of films are identical for both before and after the correction of substrate contribution to M-H data.

Table 4.15 Coercivity (H_C), saturation magnetization (M_S), remanent magnetization (M_r), squareness (M_r/M_S) of room temperature in-plane and out-of-plane M-H hysteresis curve and effective anisotropic constant (K_{eff}) of all in-situ annealed FePtCo alloy films obtained after subtracting the substrate contribution.

Sample	Direction	H_C (Oe)	M_S (emu/cc)	M_r (emu/cc)	Squareness (M_r/M_S)	K_{eff} (erg/cc)
$(Fe_{0.4}Pt_{0.6})_{0.89}Co_{0.11}$	In-plane	73	2291	2195	0.96	1.32×10^7
	Out-of-plane	132		289	0.13	
$(Fe_{0.4}Pt_{0.6})_{0.83}Co_{0.17}$	In-plane	86	1050	447	0.43	2.60×10^6
	Out-of-plane	276		141	0.13	
$(Fe_{0.4}Pt_{0.6})_{0.72}Co_{0.28}$	In-plane	73	1637	1579	0.96	9.10×10^6
	Out-of-plane	115		144	0.09	
$(Fe_{0.4}Pt_{0.6})_{0.7}Co_{0.3}$	In-plane	70	1505	1367	0.91	8.17×10^6
	Out-of-plane	225		186	0.12	

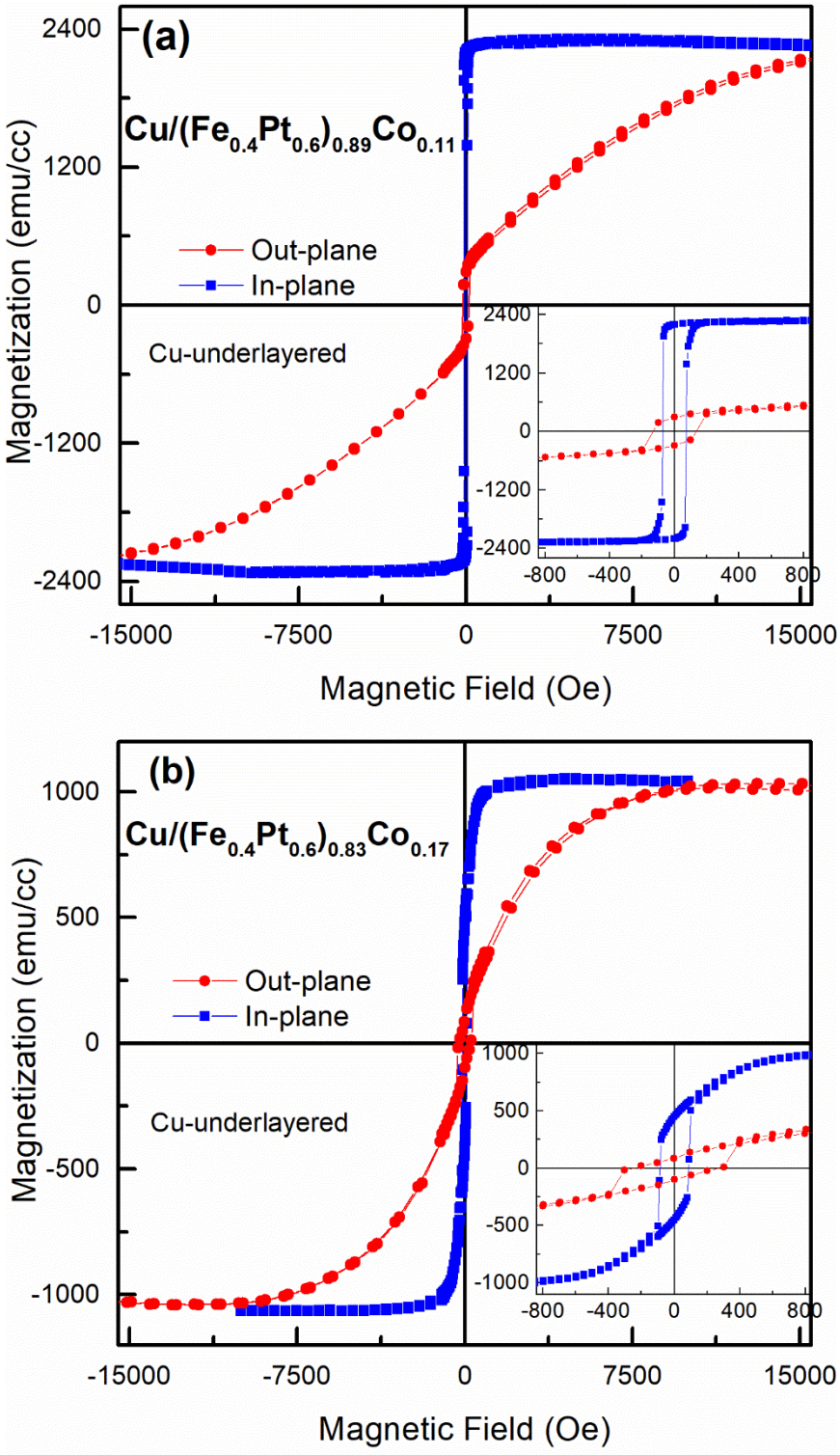

Figure 4.36 Room temperature M-H hysteresis curves of (a) 11 and (b) 17 at. % Co doped FePtCo films deposited on 2 nm Cu-underlayer.

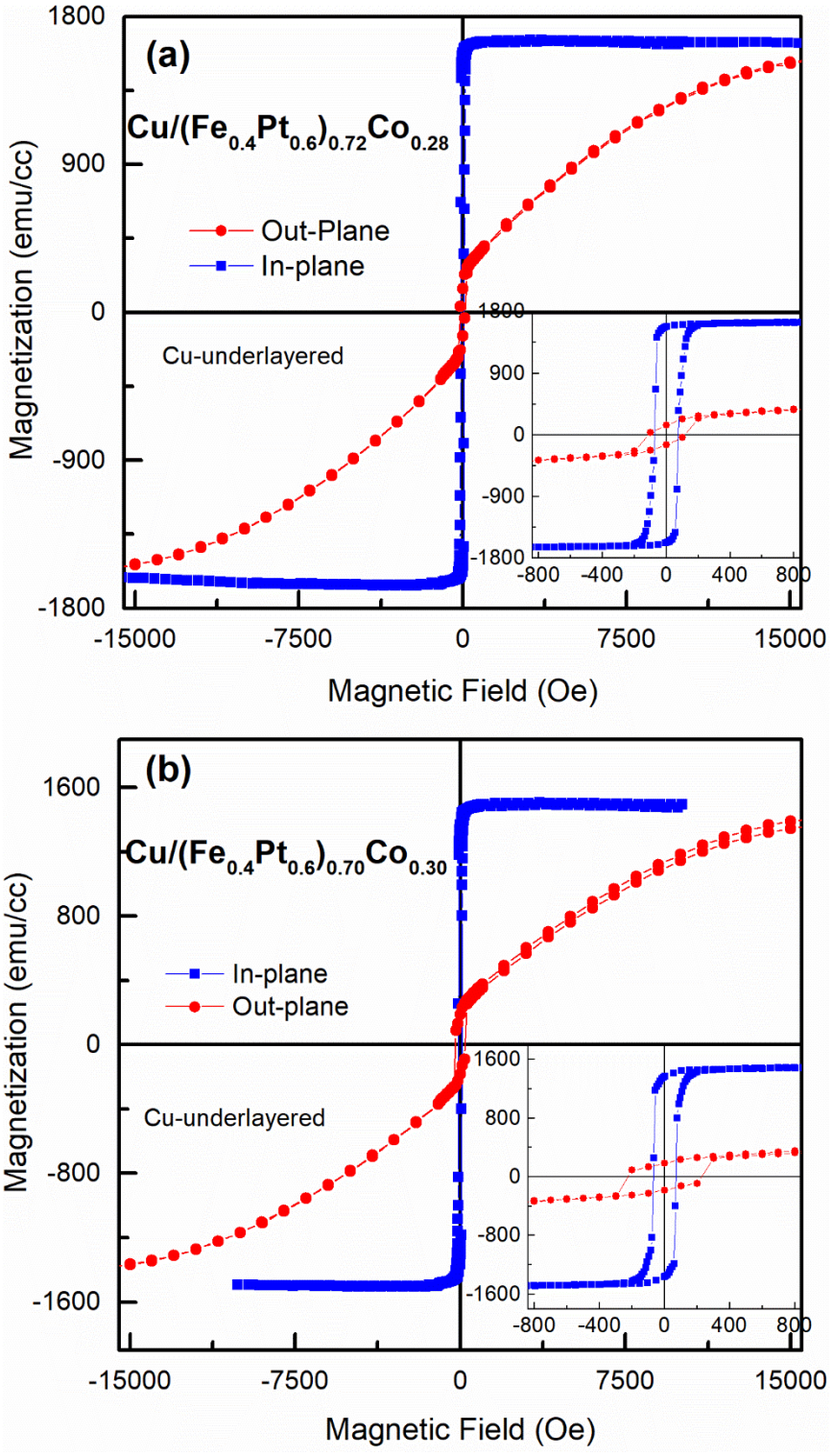

Figure 4.37 Room temperature M-H hysteresis curves of (a) 28 and (b) 30 at. % Co doped FePtCo films deposited on 2 nm Cu-underlayer.

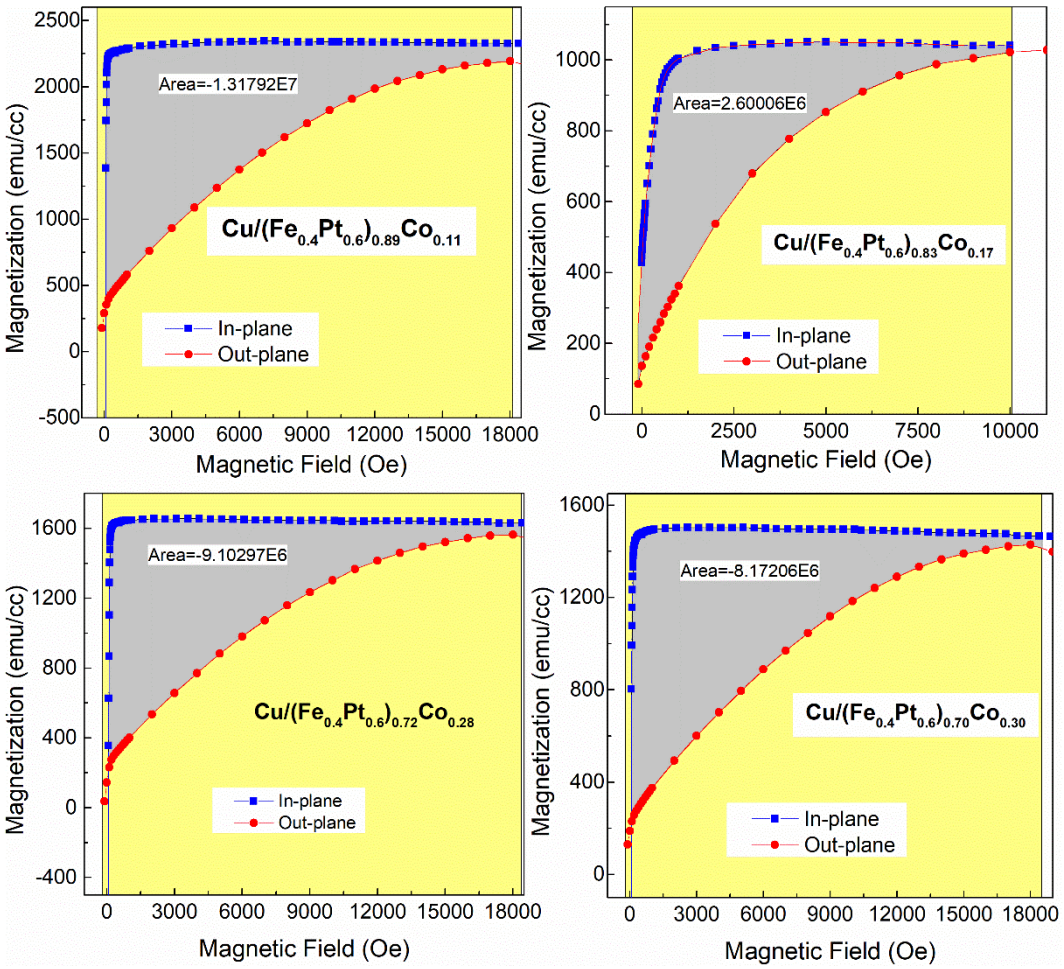

Figure 4.38 Calculation of difference in area enclosed by in-plane and out-plane M-H hysteresis loop of Cu-underlayered thin films by integration. The shaded area in grey colour represents the difference in area which is the quantitative value of K_{eff}.

The squareness of in-plane M-H loop (Figure 4.39 (c)) also varies in line of the variation of M_S and in-plane M_r. This variation is also found to be identical before substrate contribution was corrected (inset of Figure 4.39 (c)). This observation leads to drawing an inference that the films with larger M_S exhibit better squareness and smaller H_C. This suggests that for the film with larger M_S, the coercive field arises due to magnetic reversal by domain wall nucleation, and for those films with smaller M_S, large coercivity arises due to irreversible spin rotation as described by Swerts *et al.* [57]. This appears that the irreversible spin rotation leads to antiferromagnetic interaction between Co and FePt sublattice due to which reduced M_S is observed with addition of Co to FePt. The coercivity, M_S and the nature of magnetic interaction in these films appears to be interdependent on each other. The

out-of-plane squareness before (inset of Figure 4.39 (c)) and after (Figure 4.39 (c)) appears to be independent of film composition as the variation with Co content is negligible as compared to the in-plane squareness. The K_{eff} first decreases with an increase in Co content up to 17 at. % then increases on further increase of Co doping. This shows that Co doping up to 17 at. % results reduction in K_{eff} due to the dominance of antiferromagnetic interaction. The observed results on M_S, M_r, M_r/M_S, and K_{eff} indicate that there is a critical Co doping concentration at which M_S, M_r, M_r/M_s and K_{eff} all become minimum. Below and above this critical value of Co content these magnetic parameters increase. On the other hand at that critical value of Co content H_C becomes maximum. Thus by doping a suitable amount of Co, the magnetic properties of this film can be tuned by inserting Cu-underlayer.

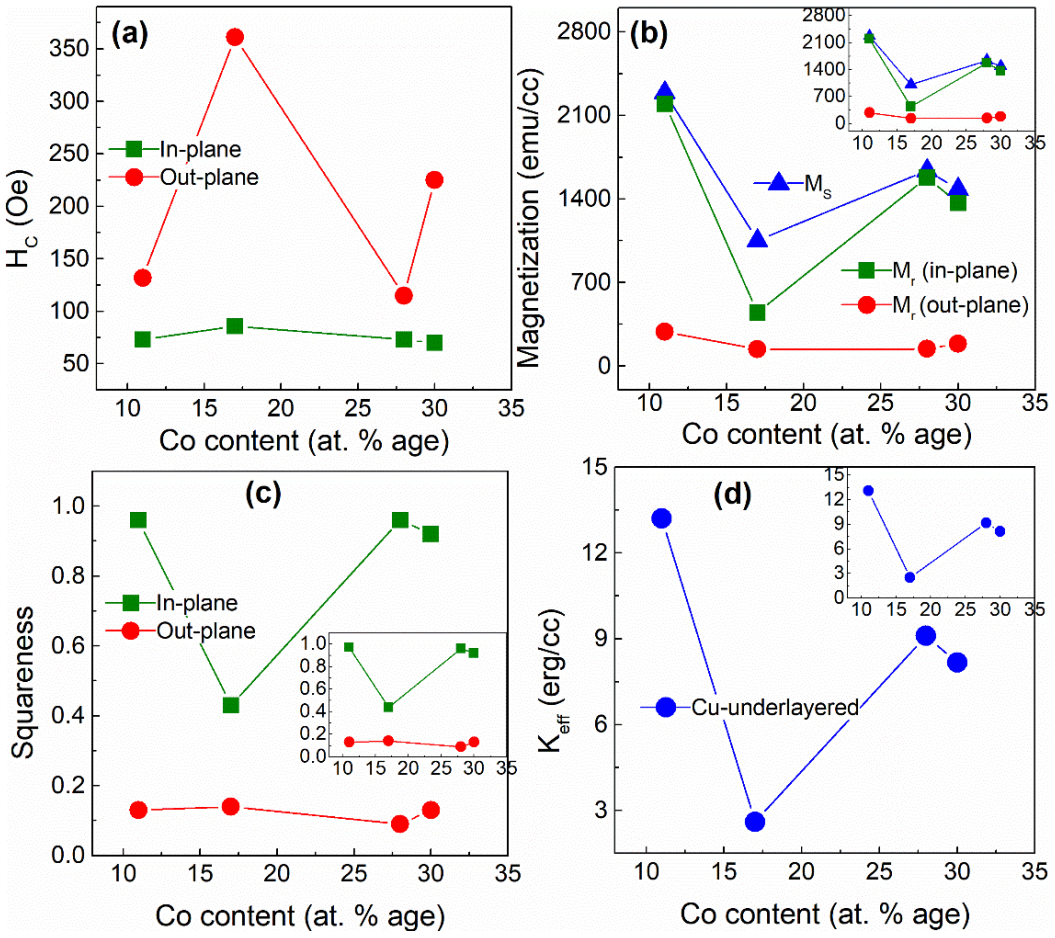

Figure 4.39 Plot of variation of (a) coercivity, (b) Magnetization, (c) squareness and (d) K_{eff} as a function of Co content of Cu-underlayered FePtCo films. The inset of figure (b), (c) and (d) represents the magnetic parameters obtained from M-H curves without subtracting substrate contribution.

4.6.4 Influence of Deposition Conditions on Magnetic Property

To analyze the influence of deposition conditions on the magnetic properties of FePtCo thin films, the obtained magnetic results obtained after correcting the substrate contribution to M-H for all prepared thin films under three conditions are plotted in Figure 4.40 (a)-(f). The as-deposited thin films possess smaller in-plane H_C than annealed and Cu-underlayered films as shown in Figure 4.40 (a). The annealed and Cu-underlayered films have nearly the same in-plane H_C for the same film composition. This shows that annealing and insertion of Cu-underlayer help to enhance in-plane H_C over as-deposition. However, with increase in Co doping the in-plane H_C of all films deposited under three conditions approach each other which can be clearly seen in Figure 4.40 (a) for 30 at. % Co doped film. A different result is observed for out-of-plane magnetization as shown in Figure 4.40 (b). As-deposited pure FePt film has larger out-plane H_C than annealed film. However, 11 at. % Co doped film deposited under annealed condition possesses the exceptionally largest out-plane H_C out of all prepared films. For higher Co content films above 17 at. % Cu-underlayered films are found to have larger out-plane H_C. The annealing of films is found to enhance the magnetization over as-deposition for pure FePt and 11% Co doped films. For other films, M_S of annealed films is smaller than the M_S of as-deposited and Cu-underlayered films. The variation of M_S of Cu-underlayered films with Co content is found to be similar to that of annealed films. However, Co doped Cu-underlayered films possess the largest M_S for films with the same composition except film with 17 at. % Co as seen in Figure 4.40 (c). This indicates that insertion of Cu-underlayer is effective in tuning the magnetization. The deep in M_S versus Co content curves for 17 % Co films prepared under annealing and Cu-underlayerd represent the existence of strong antiferromagnetic interaction between Co and FePt sublattice. It is also seen that with increase in Co doping the M_S-Co content curves approach each other as observed for variation of in-plane H_C. The M_r of in-plane magnetization shows a similar variation as that of variation of M_S. The annealing of films enhances the in-plane M_r pure FePt and 11% Co doped film over as-deposition. Above 11 at. % Co, the annealed films possess least M_r as compared to the as-deposited and Cu-underlayered films. On the other hand, Co doped Cu-underlayered films possess largest in-plane M_r except

for 17 at. % Co. This again shows that insertion of Cu-underlayer of suitable thickness will help M_r to increase. A deep in M_r versus at. % age of Co content curved at 17% is observed in both annealed and Cu-underlayered films as can be seen in Figure 4.40 (c). This is due to the strong antiferromagnetic coupling between Co and FePt sublattice which results in a reduction of M_r along with M_S of in-plane magnetization. All films prepared under three deposition conditions are found to possess comparatively smaller out-plane M_r and show small variations in a similar pattern as a function of Co content. All Cu-underlayered films show slightly greater M_r than as-deposited and annealed films of same composition. The as-deposited films show an overall decreasing out-plane M_r and have smaller out-plane M_r than annealed and Cu-underlayered films except pure FePt film. On the other hand, annealed films show random variation in out-plane M_r with Co doping with M_r values in between the M_r of as-deposited and Cu-underlayered films. The annealed pure FePt film possesses the least out-plane M_r of all the prepared films. From Figure 4.40 (e), it can be seen that the as-deposited films show an overall increase of in-plane squareness but have an overall decreasing out-plane squareness of M-H loop with an increase in Co content. The annealed films on the other hand have an overall decreased in-plane squareness and overall increasing out-plane squareness with Co doping. The Cu-underlayered films also show better squareness of M-H loop both in in-plane and out-plane direction except 17 at. % Co doped film. Due to the small M_r the 17 at. % Co film has the smallest in-plane squareness out of all films. The plot of compositional variation of K_{eff} of all films prepared under three deposition conditions are presented in Figure 4.40 (f). The figure shows that the K_{eff} of as-deposited films varies in an identical manner as that of M_S of as-deposited films. The pure FePt and 17 at. % Co doped as-deposited films possess largest K_{eff} than the films with same composition deposited in other conditions. On the other hand, the K_{eff} of annealed films varies with Co content in a more random pattern. The nature of variation is found to be similar as the variation of M_S and in-plane M_r. The K_{eff} of Cu-underlayered films also varies in a similar pattern as observed for M_S and in-plane H_C and can also be resembled with the variation of K_{eff} of annealed films. Except for 17 at. % Co, other Cu-underlayered films exhibit in-plane magnetic anisotropy of largest K_{eff} of all Co doped films prepared under as-

deposition and annealed conditions. The deep in the M_S and K_{eff} curves at 17 at. % Co annealed and underlayered films is attributed to the existence of strong antiferromagnetic interaction. The results indicate that the film deposition condition plays a significant role in controlling the magnetic properties of these class of materials.

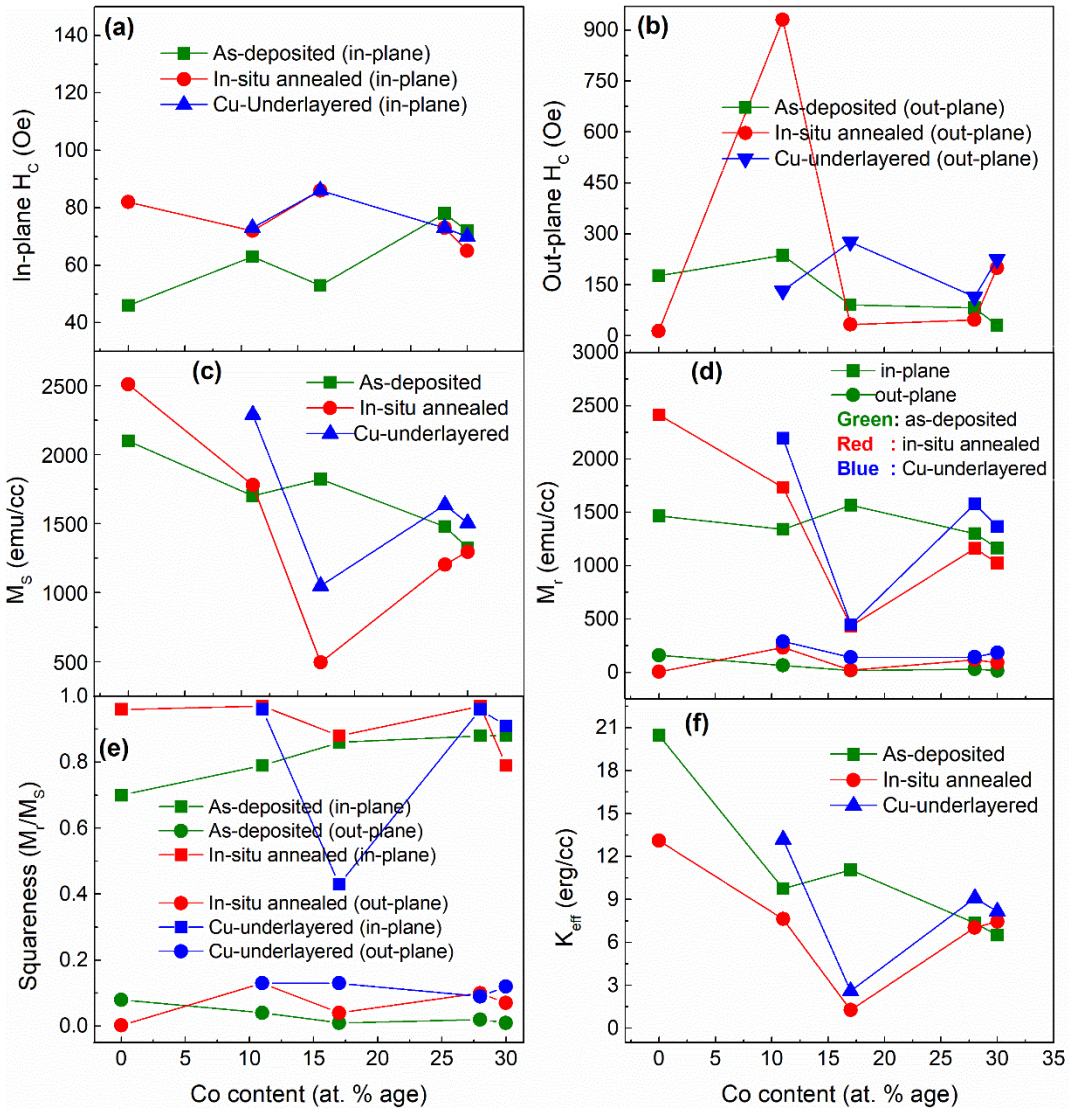

Figure 4.40 Plot of variation of (a) in-plane H_C, (b) out-plane H_C, (c) M_S, (d) M_r, (e) squareness and (f) K_{eff} as a function of Co content of FePtCo films deposited under three conditions.

Several studies were reported on substitutional doping of TM elements such as Cu, Mn, Ni, Cr etc, in which the FCC A1 phase of FePt films were transformed to L10 ordered FCT structure by annealing or by depositing at elevated substrate

temperatures [5,87,118–120,127,128,135,137,138]. In these studies, though ordering temperatures and T_C were successfully reduced by third element doping, the K_u and M_S of the films were substantially reduced. The present thesis work reveals that the in-situ annealing of films can increase M_S and in-plane M_r of films with small percentage of Co. On the other hand, insertion of Cu-underlayer of 2 nm thickness is proven to increase the H_C, M_S, M_r as well as K_{eff} for certain at. % Co-doped FePt thin films. Moreover, all the samples deposited under all three deposition conditions under study crystallize in chemically disordered FCC structure showing (111) texture and exhibit soft ferromagnetism. However, in-situ annealing of films at 673 K and insertion of 2 nm Cu-underlayer do not result structural phase transition from FCC to chemically ordered structure. This indicates that structural ordering temperature for these films lies above 673 K. These results are in agreement with the reported results of other third element doped FePt based thin films cited in chapter 1.